Diffusion-weighted MRI in neurodegenerative and psychiatric animal models: experimental strategies and main outcomes

Amr Eed[1], Antonio Cerdán Cerdá[1], Juan Lerma[1], Silvia De Santis[1,2]

[1]Instituto de Neurociencias, CSIC/UMH, San Juan de Alicante, Alicante, Spain.
[2]CUBRIC, School of Psychology, Cardiff University, Cardiff, UK

Corresponding: Silvia De Santis, dsilvia@umh.es

Abstract

Preclinical MRI approaches constitute a key tool to study a wide variety of neurological and psychiatric illnesses, allowing a more direct investigation of the disorder substrate and, at the same time, the possibility of back-translating such findings to human subjects. However, the lack of consensus on the optimal experimental scheme used to acquire the data has led to relatively high heterogeneity in the choice of protocols, which can potentially impact the comparison between results obtained by different groups, even using the same animal model. This is especially true for diffusion-weighted MRI data, where certain experimental choices can impact not only on the accuracy and precision of the extracted biomarkers, but also on their biological meaning. With this in mind, we extensively examined preclinical imaging studies that used diffusion-weighted MRI to investigate neurodegenerative, neurodevelopmental and psychiatric disorders in rodent models. In this review, we discuss the main findings for each preclinical model, with a special focus on the analysis and comparison of the different acquisition strategies used across studies and their impact on the heterogeneity of the findings.

Introduction

Magnetic resonance imaging (MRI), a technique widely used in the clinical practice as a diagnostic tool, has revealed a fundamental importance as a powerful, non-invasive analysis tool also in animal studies and, more specifically, in preclinical pharmaceutical research. The development of high field scanners (e.g. 7T) has significantly improved the spatial resolution, granting access to the investigation of small animals like rodents. Indeed, in recent years, knock-out or transgenic mice, where specific genes have been removed or altered, have been widely used in fundamental research. The combination of these models with this powerful imaging technique can shed light onto how genetic alterations derived into pathologies. Because of its non-invasiveness, MRI allows repeated observations on the same subject as well as longitudinal studies and is being increasingly used in rodent models of brain diseases.

The landscape of MRI can widely be divided into two major areas: structural and functional. Structural MRI is mainly concerned with conveying information about the underlying tissue properties, while patterns of brain activity can be measured and compared using functional contrasts. Structural contrasts such as T_1 and T_2 are suited for mapping brain anatomy and hence are widely used in clinical investigation to extract key information such as cortical thickness and the volume of different anatomical structures. Conversely, functional contrasts are meant to catch the brain in action. Sensitizing the machine to events such as blood oxygenation or blood flow is the basis for blood oxygenation level-dependent and cerebral blood flow functional MRI.

Diffusion weighted MRI (dw-MRI) belongs to the structural domain (see Huettel et al., 2014 for a review about the different contrasts), but it stands out due its ability to extract information about the microstructural properties (as in the range of microns) of the tissue in contrast with millimeters level other structural modalities work on.

Amongst the different contrasts available, dw-MRI is widely used to study the brain and brain-related pathologies. This review examines the experimental procedures used to infer structural differences in murine neurodegenerative, neurodevelopment and psychiatric models versus wild type animals. The manuscript is structured as follows. First, we briefly explain the fundaments of dw-MRI and introduce the different parameters that define the acquisition scheme. We then describe the most popular model used to fit the diffusion signal, the diffusion tensor imaging (DTI), along with some of the most used advanced models. After introducing the state-of-the-art of preclinical

modelling, we highlight the relevant aspects that hamper the results homogeneity and, ultimately, the transference to the clinic. The body of this article consists of an overview of the different experimental strains and preparations, dw-MRI acquisition parameters, biophysical models, and main results that where reported so far using dw-MRI to characterize the most common pathologies of the central nervous system.

Diffusion-weighted MRI: theory, experimental scheme, and biophysical models

Dw-MRI contrast is sensitive to the random displacement of water molecules, which in biological tissues is constantly hindered by the presence of barriers in the form of cell membranes and other organelles inside the cell. By probing the path water molecules follow while diffusing, important characteristics of the underlying microstructure can be measured (see Jones 2010, Emsell et al., 2016).

Sensitizing the MRI signal to diffusion usually requires a diffusion-sensitized acquisition sequence; the pulsed gradient spin echo (PGSE) is the most common (Stejskal and Tanner 1965). The measured signal is an exponential decay defined as follows:

$$S = S_0 \cdot e^{-bD} \quad (1.1)$$

Where:

$$b = \gamma^2 G^2 \delta^2 \left(\Delta - \frac{\delta}{3}\right) \quad (1.2)$$

S_0 represents the signal in absence of diffusion weighting, S is the signal, D is the diffusion coefficient of the water molecules, γ is the gyromagnetic ratio, G is the strength of the gradient applied, δ is gradient duration, and Δ is the time difference between the two gradient pulses. The diffusion time Δ describes the amount of time the water molecules are allowed to displace before acquiring the signal. The PGSE sequence is illustrated in Fig. 1. A typical diffusion experiment will encompass several

diffusion-weighted images along different noncollinear, non-coplanar unique directions along with one or more images acquired without gradient, serving as a reference. The amount of diffusion weighting applied is quantified by the b-value (Le Bihan and Breton 1985).

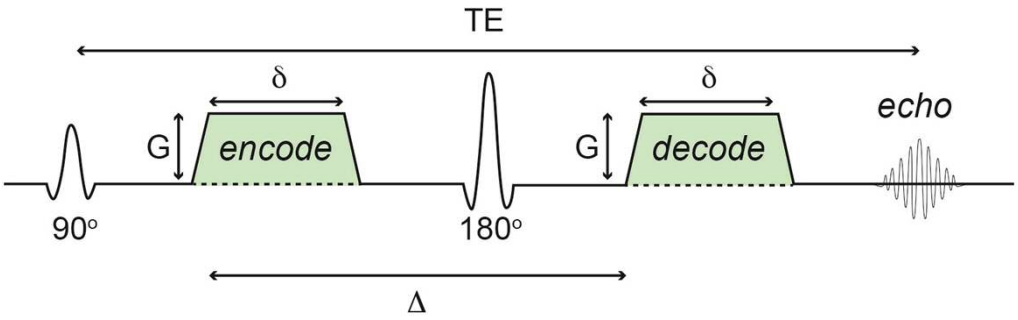

Figure 1: Pulsed gradient spin echo (PGSE) sequence. The basic PGSE sequence consists of two radio-frequency pulses, an excitation pulse (90°), a refocusing pulse (180°), and two gradient pulses (green trapezoids). G represent the strength, and δ the duration of the gradient. The diffusion time, Δ, is the time from the start of the first gradient pulse to the start of the second gradient pulse. TE is the echo time.

Since its inception by Basser et al., in 1994, diffusion tensor imaging (DTI) has gained wide acceptance as the go-to method of modelling the diffusion signal as a consequence of its simplicity, robustness, and the reasonable acquisition parameters (Basser et al., 1994). DTI uses a 3 × 3 apparent diffusion tensor to represent diffusion in 3D space (see Kingsley 2006). Multiple measures can be calculated from the diffusion tensor; the most frequently used are fractional anisotropy (FA), mean diffusivity (MD), axial diffusivity (L1), and radial diffusivity (RD) (Basser 1995).

Despite its popularity, DTI suffers from a number of limitations, the main one being that it assumes that the diffusion follows a Gaussian distribution, while the signal can also come from intracellular water molecules where restrictions generate a deviation from Gaussian behaviour (Curran et al., 2016). Numerous advanced models have been developed over the years to mend the pitfalls of the DTI model. Diffusion kurtosis imaging (DKI) quantifies the degree to which the diffusing water molecules displacement probability deviates from the Gaussian distribution, which gives a more realistic view of the diffusion in tissues like the gray matter where the non-Gaussian

diffusion is ubiquitous. The same PGSE is usually used in DKI, however, it requires higher b-values along with a larger number of gradient orientations, as the calculations are more complex than those of DTI (Jensen et al., 2005, Lu et al., 2006, Jensen et al., 2011, reviewed in Jensen and Helpern 2010).

Other approaches aim at modelling the signal as a multi-compartment model separating the contributions of the intra from extracellular compartments (see Alexander et al., 2019 for a review). The composite hindered and restricted model of diffusion (CHARMED), for instance, assumes two models of diffusion: an intra-axonal restricted diffusion, and a hindered diffusion happening elsewhere. A notable strength of such a model is that it can, to a certain degree, resolve the issue of crossing-fibers within the same voxel. A simpler approach such as neurite orientation dispersion and density imaging (NODDI) models instead the dispersion around a single fiber direction (Zhang et al., 2012).

These models have definitely enriched the insights we gain from dw-MRI by providing a more realistic view of the diffusion process more than the usual DTI. However, they require a multi-shell acquisition and higher b-values that might lead to higher noise (Alexander et al., 2019).

Animal models and dw-MRI

The recent developments in molecular biology and genome editing techniques have echoed through all fields and MRI was no exception. The ability to recapitulate human disorders using animal models opened a big window for a closer look into these diseases using the rich varieties of MRI modalities. Due to the physical gap between humans and small animals like rodents, scanning small animals require special set-ups to accommodate the smaller size. Custom coils and higher field strengths are needed in order to produce a useful resolution and an improved SNR. Other things such as anesthesia, mechanisms for head fixation to limit motion artifacts and maintaining the animal's core temperature and respiration rate also often require special attention and maintenance.

A major roadblock in the face of moving dw-MRI more into the clinic is the lack of solid validation of the pathological correlates of the changes frequently elucidated by imaging. Histological samples obtained posthumously from patients are rarely available and hard to get. Using animal models comes in handy in such cases, where the post-

MRI histological examination is becoming mainstream. Using immunohistochemical techniques, things such as axons demyelination, β-amyloid accumulation, and changes in cell morphology can be investigated, quantified, and further linked to the dw-MRI findings, establishing a framework to understand the meaning of the variations in the imaging contrast (Oguz et al., 2012). These advantages do not come without a cost. Due to the evolutionary gulf between humans and rodents, these models cannot recapitulate all the aspects of a given disorder; instead, they can be thought of as a representation of a certain aspect of the disease and hence caution should always be employed when interpreting or extrapolating such findings to human studies (Jones 2010). In addition, correlating histological and imaging findings has its own shortcomings, like the difficulty of matching images between the two modalities (Horowitz et al., 2015).

Another important issue to take into account when looking at preclinical dw-MRI results and their translatability to humans, is the lack of a homogeneous strategy for designing the experimental protocol. While some parameters mostly impact on the SNR, others affect the range of diffusion on which the study is focusing. Specifically, changing the diffusion time Δ might shift the sensitivity of the analysis from mostly extracellular water to restricted water. Similarly, a high b-value will give more information about compartment undergoing slower diffusion compared to lower b-values (Assaf et al., 2008). In addition, both high Δ and high b-values will translate into a lower SNR, potentially affecting the sensitivity to changes (Hagmann et al., 2006). Also the choice of the biophysical model used to analyze the data impacts on the results, where more advanced models can increase both sensitivity and specificity to changes compared to DTI (De Santis et al., 2017). Finally, the number of unique orientations determines the accuracy and the precision of the obtained parameters and generally, a number below 20-30 is considered suboptimal (Jones and Basser 2004).

To assess the homogeneity of the results and the employed experimental protocol across studies, we searched the PubMed website for preclinical studies using dw-MRI to investigate neurodegenerative or neurodevelopmental disorders and employing rodents. Entrez tool from the Biopython library was used to scrape the website (git repository: https://github.com/amrka/pubmed_scrape_dw-MRI_preclinical). A combination of terms was used in the search including, "diffusion tensor imaging AND mice", “diffusion tensor imaging AND rats", "diffusion tensor imaging AND ferrets", "diffusion MRI AND mice", "diffusion MRI AND rats", and "diffusion MRI AND ferrets". The unique hits were refined manually in order to remove irrelevant articles.

We only included results reported by the authors which reached statistical significance, regardless of the analysis or the statistical methods used. A summary of the disease, the model used, acquisition parameters, and the most relevant results can be found in Tables 1-2, and the main experimental parameters are plotted for the different diseases investigated in Figure 2.

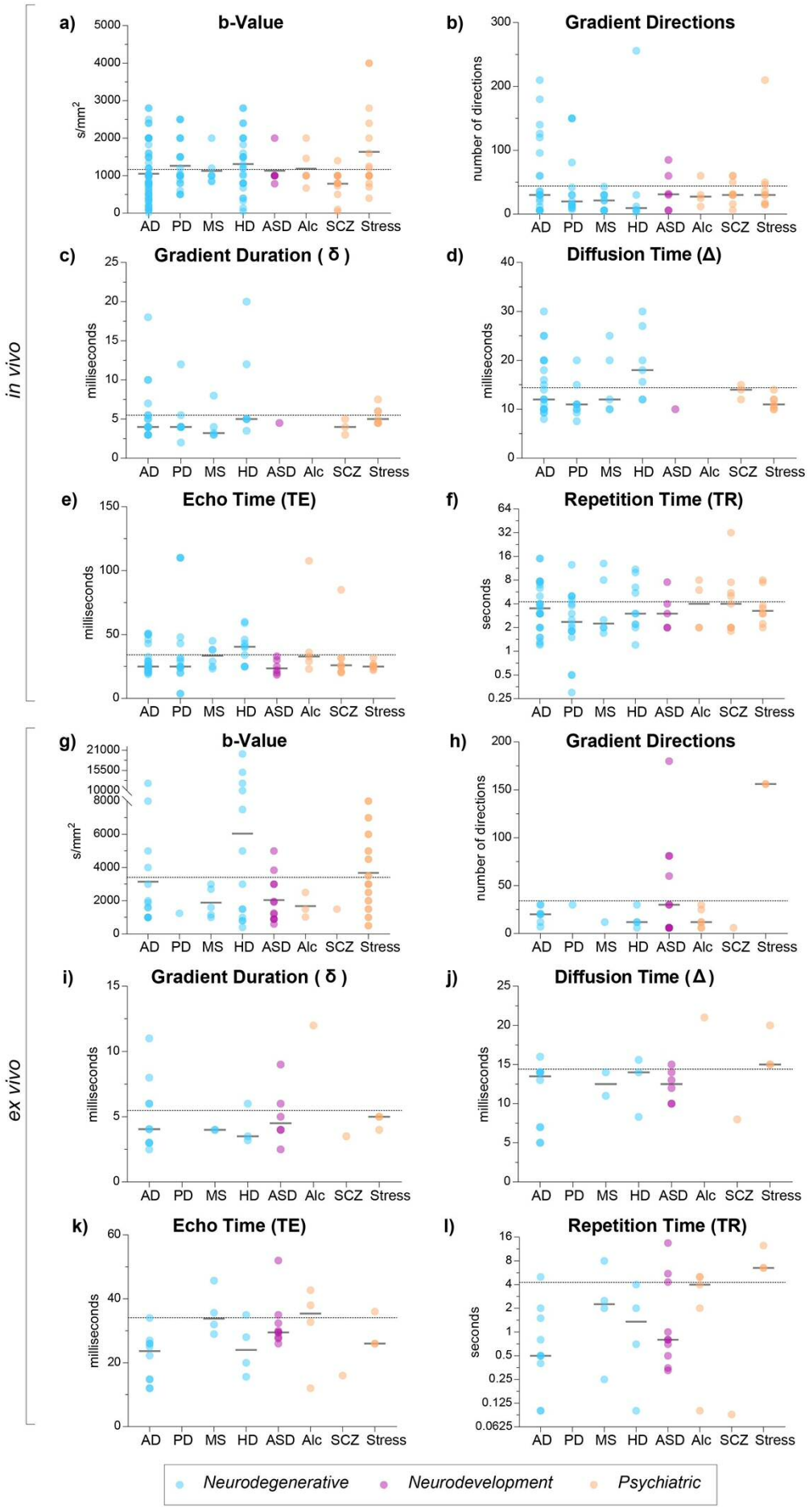
in vivo
ex vivo
a) b-Value
s/mm²
b) Gradient Directions
number of directions
c) Gradient Duration (δ)
milliseconds
d) Diffusion Time (Δ)
milliseconds
e) Echo Time (TE)
milliseconds
f) Repetition Time (TR)
seconds
g) b-Value
s/mm²
h) Gradient Directions
number of directions
i) Gradient Duration (δ)
milliseconds
j) Diffusion Time (Δ)
milliseconds
k) Echo Time (TE)
milliseconds
l) Repetition Time (TR)
seconds
AD PD MS HD ASD Alc SCZ Stress
Neurodegenerative
Neurodevelopment
Psychiatric

Figure 2. Dw-MRI parameters used in Neurodegenerative (blue), Neurodevelopment (purple) and Psychiatric (orange) preclinical models *in vivo* **(a-f)** and *ex vivo* **(g-l)**. Each plot represent one dw-MRI parameter: **(a,g)** b-Value; **(b,h)** number of noncollinear, non-coplanar gradient directions; **(c,i)** gradient duration, δ; **(d,j)** diffusion time, Δ; **(e,k)** echo time, TE; **(f,l)** repetition time, TR. The dashed line represents the mean parameter value calculated across all included articles. The narrow continuous line represents mean in specific neuropathology. Dots represent the corresponding parameter values used in each article. Abbreviations: AD=Alzheimer's disease; PD=Parkinson's disease; MS=Multiple sclerosis; HD=Huntington's disease; ASD=Autism spectrum disorder; Alc=Alcoholism; SCZ=Schizophrenia.

Neurodegenerative diseases

Diseases such as Alzheimer's, Parkinson's, Huntington's, and multiple sclerosis together represent the most prevalent neurodegenerative disorders, with a total burden of 23% of the disability-adjusted life years, which is expected to further grow by 2030 (World Health Organization). The deposition of misfolded Amyloid-β (Aβ) plaques between nerve cells and tau neurofibrillary tangles inside the neurons are the most prominent hallmarks of Alzheimer's disease (AD); such aggregation starts a cascade of events, involving inflammation, neuronal and synaptic degeneration, and formation of tau neurofibrillary tangles, that eventually leads to cognitive deterioration (Small and Duff 2008). AD has been linked to mutations in genes responsible for the formation and cleavage of Amyloid-β such as amyloid precursor protein (*APP*), γ-secretase proteins presenilin 1 (*PSEN1*), and presenilin 2 (*PSEN2*) (Small and Duff 2008). Other genetic risk factors such as *APOE* and *TREM2* genes have been linked to sporadic and early-onset forms of AD (Scheltens et al., 2016).

Being unique to humans, finding an effective animal model that recapitulates the entire biology of AD remains elusive; genetically modified mice engineered to overexpress APP are an important tool, but replicate only one aspect of the disorder (Drummond and Wisniewski 2017). The majority of the articles examined for this review used APP/PSEN1 mouse model with APP gene carrying the Swedish double mutation (KM670/671NL) and PSEN1 with one type of mutations such as L166p (Vanhoutte et al., 2013) or ΔE9 (Qin et al., 2013). A preponderance of studies using

models with APP harboring the Swedish double mutations (Tg2576) with no PSEN1 mutations was still observed (Harms et al., 2006). Both kinds of models give rise to amyloid deposition in various brain structures but differ in the time course of such deposition. Other models incorporate other mutations aiming to better replicate the disorder by allowing the formation of tau-neurofibrillary tangles such as the triple transgenic (3xTg) model (Snow et al., 2017). Not surprisingly, the mouse was the animal of choice occupying the biggest chunk of the literature with a few articles settling for using rats instead (Munoz-Moreno et al., 2018, Anckaerts et al., 2019). Owing to the rodents' small-sized brains, a strong magnetic field is mandatory. Field strengths between 4.7 T to 11.7 T were employed in all the studies.

FA, MD, L1, and RD are the most commonly reported scalar measures whether in region of interest (ROI), voxel-based (VBA) type of analysis, or both. Results showed a good agreement between studies regardless of the model used, the acquisition parameters, or the type of the analysis. Most studies reported a decrease in FA accompanied by an increase in MD in white matter structures such as the corpus callosum, fornix, internal capsule, and external capsule as well as in gray matter tissues including the hippocampus, large parts of the cortex, and the thalamus (Fig. 3a) (Shu et al., 2013, Qin et al., 2013). Using the same model and similar acquisition parameters with slightly younger animals, Zerbi and coworkers showed a voxel-wise increase in MD in the fimbria and the hippocampus, but lower MD in the body of the corpus callosum, the fornix, and the cerebral peduncle (Zerbi et al., 2013). This discrepancy cannot be explained by different amyloid deposition patterns. Interestingly, Zerbi et al. used a b-value of 1000 s/mm^2, while Qin and Shu et al. chose a b-value of 800 s/mm^2. This slight difference can translate into a better SNR, but also a different sensitivity to hindered versus restricted compartments. A staggering amount of human studies seems to be in accordance with the former results (see for example Stahl et al., 2007, Zhang et al., 2007, Agosta et al., 2011, Shu et al., 2011). Post-mortem literature reported alterations in the microstructure in various brain tissues, including loss of myelin, cellular death, and neurodegeneration. Such alterations affect the structural integrity and can be the cause behind the decrease in FA values and the increase in MD, respectively. Intriguingly, the results from applying advanced models seem to corroborate these findings. Using DKI, some studies have reported an increase in all three of DKI metrics (axial kurtosis (AK), mean kurtosis (MK), and radial kurtosis (RK)) in parts of the cortex, whilst they did not report any change in those metrics in the hippocampus or any

of the white matter main tracts (Vanhoutte et al., 2013, Praet et al., 2018). One interpretation might be that DKI is sensitive to certain aspects of the underlying abnormalities that DTI metrics are impartial to. Using NODDI on an animal model of tau pathology, a strong correlation between the tau burden in the cortex and hippocampus and the neural density in these structures has been found (Colgan et al., 2016). Such correlations might hint at a sensitivity of NODDI metrics towards tau-related pathology, however, the results are quite limited by the small sample size.

RD and L1 are fairly reported alongside FA and MD with no general consensus on the direction of the changes in the different structures. A longitudinal study showed a decrease in RD values at 12 months, then reported an increase in these values at 16 and 18 months (Sun et al., 2005). However, as elegantly demonstrated by Wheeler-Kingshott et al., the lax usage of the L1 and RD should be discouraged especially in regions such as the gray matter where crossing fibers are ubiquitous (Wheeler-Kingshott and Cercignani 2009).

A progressive loss of dopaminergic neurons in the substantia negra (SN) and together with the deposition of a misfolded protein called α-synuclein intracellularly, forming the Lewy bodies, constitutes the cardinal hallmarks of Parkinson's disease (PD) (Poewe et al., 2017). Unlike AD, the majority of PD incidents are idiopathic with a marginal number of cases that can be attributed to heritable factors or exposure to environmental toxins (Nalls et al., 2014, Ascherio and Schwarzschild 2016). Creating an effective animal model of PD that embodies the disorder's pathophysiology remains elusive (Beal 2010) with most of the studies settling for the traditional toxin-treated models. Toxins such as 6-hydroxydopamine (6-OHDA), rotenone, and 1-methyl-4-phenyl-1,2,3,6-tetrahydropyridine (MPTP) were unilaterally injected either directly in the SN itself (see, for example, Liu et al., 2017), the striatum (Perlbarg et al., 2018), or the medial forebrain bundle in a few studies (Monnot et al., 2017). Interestingly, PD studies witnessed a surge in using rats, rather than mice, as the animal of choice, probably to facilitate performing the surgeries of the intracranial injection. A few studies used transgenic mice or rats harboring mutations that were linked to the familial form of PD in humans, such as TNWT-61 transgenic mice that overexpress α-synuclein (Khairnar et al., 2015, Khairnar et al., 2016, Khairnar et al., 2017), or rat models featuring a knock-out of *PINK1*, as it has been implicated in cases of familial early-onset parkinsonism (Ferris et al., 2018). Despite the recapitulation of some of the hallmarks of PD, these models lack the neurodegeneration of the dopaminergic neurons,

limiting their potential to symptomatic research. Perhaps the most interesting animal model would be the one known as the MitoPark mouse, which faithfully mimics most of the hallmarks of PD including the progressive neurodegeneration; however, the fact that it is not built on a human genetic mutation limits its potential (Beal 2010).

Unfortunately, due to the variation in the substance injected, doses, and site of injection, comparing the results between different studies is quite challenging (Table 1). The SN as the structure associated the most with PD, showed different values of DTI scalar metrics across different studies (Fig. 3b). Using models of both 6-OHDA and rotenone, Liu et al. reported an immediate FA decrease in the SN, followed by an increase six weeks after the injection in comparison with the sham controls (Liu et al., 2018a), while a persistent decrease after one and six weeks was also reported (Fang et al., 2018). This decrease in FA was also observed in the MitoPark animals (Cong et al., 2016).

A number of studies used DKI to investigate TNWT-61 animal model at different stages. Many structures showed an increase in all three kurtosis measures (MK, AK, RK). The changes in the SN, ipsilaterally to the injection, start as early as six months of age, while they can appear by three months in regions such as the striatum (Khairnar et al., 2015, Khairnar et al., 2016, Khairnar et al., 2017). These findings might favor the DKI metrics as more sensitive measures than the DTI ones that could have the potential to serve as an early diagnostic tool.

Huntington's disease (HD) emerges from a mutation in the *HTT* gene that encodes for a protein of unknown function called Huntingtin. The mutated form of Huntingtin protein tends to have a toxic effect on neurons, especially the striatum's medium spiny neurons. This toxicity is usually manifested as motor as well as cognitive and behavioral symptoms (Bates et al., 2015). The understanding of the molecular background of HD is very well reflected in the rodent models used to study the illness. All the models have an *HTT* gene featuring a different number of CAG repeats, the very same repeats associated with the disease in humans (Blockx et al., 2012a, Teo et al., 2016, Gatto et al., 2019). The use of transgenic rat model (TgHD) was quite common in giving this model an edge due to the brain size and the possible enhanced SNR (Table 1). The homogeneity of the molecular background of the models was also evident in terms of the results. Even though there was a wide gap in the ages of the animals used, the results seemed to be in accordance with each other. The values of FA in all the articles that reported a significant change in the corpus callosum or its various sub-

components were found to be decreased with the respect to the control animals (Chyi and Chang 1999, Xiang et al., 2011, Garcia-Miralles et al., 2016, Teo et al., 2016, Gatto et al., 2019), while this was reversed in some of the gray matter structures such as the striatum (Fig. 3c) (Blockx et al., 2012b, Antonsen et al., 2013). Using a simple acquisition protocol of only one shell of 800 s/mm^2 and 6 directions, Blockx et al. failed to unearth any differences (Blockx et al., 2011), whilst using a multi-shell acquisition of severn shells, they reported numerous significant in changes (Blockx et al., 2012a, Blockx et al., 2012b).

Multiple sclerosis (MS) is a severe disease which causes demyelination and axonal damage, both focally and globally (Filippi et al., 2018). Due to the poorly understood etiology, the available animal models poorly recapitulate the disorder such that the demyelination in those models is induced while the MS has a spontaneous onset (Rice 2012). The most popular model is what is called experimental autoimmune encephalomyelitis (EAE) where the animals are immunized with a myelin antigen to harness the immunity to attack its own myelin (Rice 2012). The other available models feature toxic demyelination, where the animals are is that toxic to the oligodendrocytes such as cuprizone.

The literature reviewed used exclusively the EAE (Nishioka et al., 2017, Crombe et al., 2018) or the cuprizone model (CPZ) (Song et al., 2005, Atkinson et al., 2019), while one article experimented with a mixed model of both worlds (Boretius et al., 2012). As expected, a diminished FA was observed in the corpus callosum and, more importantly, in the optic nerve and the optic tracts (Fig. 3d) (Sun et al., 2007, Nishioka et al., 2017, Nishioka et al., 2019) recapitulating an important feature of MS in humans where patients suffer from visual deficits (Table 1). A significant difference in the MD values between MS models and their corresponding control was reported only twice (Crombe et al., 2018, Atkinson et al., 2019). Both studies used reasonable acquisition protcols consist of two shells and a sufficient number of directions. Factors such as different diffusion time and spatial resolution might be in play in such adverserial results. Diffusion times of 12 ms with a resolution of 82 × 81 × 203 μm^3 (Crombe et al., 2018), 10 ms with resolution of 156 × 156 × 1000 μm^3 (Atkinson et al., 2019) have been reported. Despite the gain in SNR, the lower resolution used in this latter study makes the partial volume effect a real concern here.

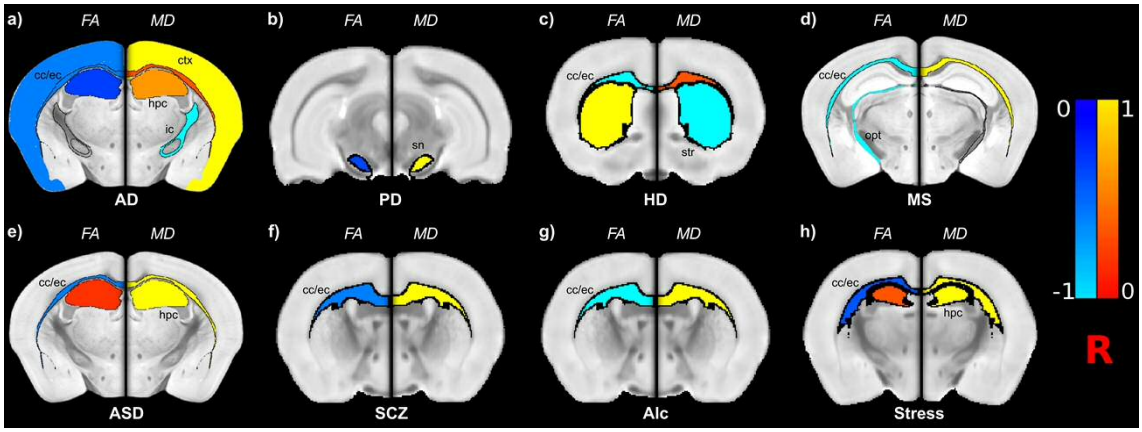

Figure 3. Visual representation of the number of studies reporting increase (in red) and/or decrease (in blue) in FA and MD in neurodegenerative (a-d) and neurodevelopmental and mood disorders (e-h) in the most affected structures. Results are overlaid on a high-resolution template of a mouse brain (a, d, e) or a rat brain (b, c, f, g, h) depending on which animal model is used more frequently in each disease. Results are calculated as ((# of studies reporting an FA or an MD increase - # of studies reporting an FA or an MD decrease) / total # of studies). FA results are displayed on the left hemispheres and MD results are displayed on the right hemispheres. We used the AMBMC MRI mouse brain template and atlas (Richards et al., 2011, Ullmann et al., 2013, Ullmann et al., 2014, Janke and Ullmann 2015) and the SIGMA MRI rat brain template and atlas (Barrière et al., 2019). **Abbreviations:** FA, fractional anisotropy; AD, Alzheimer's disease; Alc, Alcoholism; ASD, Autism spectrum disorder; cc/ec, corpus callosum/external capsule; ctx, different parts of the cortex; HD, Huntington's disease; hpc, hippocampus; ic, internal capsule; MD, mean diffusivity; MS, multiple sclerosis; opt, optic tract; PD, Parkinson's disease; R, right; SCZ, schizophrenia; sn, substantia nigra; str, striatum.

Neurodevelopmental and psychiatric disorders

While preclinical models of neurodegenerative disorders have a long tradition in biomedical research, more recently imaging techniques have been applied also to look at subtle changes in psychiatric and neurodevlopmental animal models. Autism spectrum disorders (ASD) describe a myriad of heterogeneous neurodevelopmental disorders characterized by ill-forms of communication with others, the pervasiveness of repetitive behaviors, and social disinterest (Miles 2011). A growing body of evidence

defined the genetic component, rather than the environmental, to be the major cause behind ASD. Genome-wide association studies (GWAS) studies have identified a number of genes associated with a high risk of developing ASD such as *ANK2*, *ARID1B*, *CACNA2D3*, *FOXP1, GRIK4*, and *GRIN2B* (Iossifov et al., 2014). Such mutations inspired the development of animal models trying to recapitulate the essence of ASD. However, interpreting such results must be put in the context of the uniqueness of the disorder to humans.

Due to the heterogeneity that comes with ASD, our search highlighted the usage of various models aiming at recapitulating different mutations, with a limited number of articles using the same model. Such a limitation made it challenging to compare the models to each other. However, some global patterns were observed (Table 2). The majority of the articles reported a decrease in FA in WM structures such as the corpus callosum, the external capsule, the fornix, and the anterior commissure (for instance, Ellegood et al., 2011, Dodero et al., 2013, Zerbi et al., 2019) as well as some other GM tissues such as the hippocampus, the cerebellum, and the thalamus (Fig. 3e) (Ellegood et al., 2011). This decrease was accompanied in some cases with an increase in RD or other scalar metrics. The opposite change in FA and RD, albeit to a lower extent, was also reported. In his longitudinal study, for instance, Kumar et al. reported a trend of increasing FA values in the corpus callosum that peaked at P70 where compared to a cross-sectional control, was significantly different (Kumar et al., 2012). This could hint at a change in the model throughout its lifetime reminiscent of the ASD in humans as briefed earlier. Such a discrepancy can emanate from a multitude of factors, not least of all the very nature of ASD rather than the models themselves, or can be attributed to poor acquisition protocols, where most of the literature reported the use of only 6 directions which, potentially, can lead to a poor tensor estimation (Ellegood et al., 2011, Kumar et al., 2012, Kumar et al., 2014, Kumar et al., 2018, Pervolaraki et al., 2019). Another prominent drawback in the literature analyzed is the dominant use of male animals in most of the studies (Kumar et al., 2014, Wilkes et al., 2019).

Aside from the direction of the change in FA and RD, these articles seem to agree on a change in the microstructure of the white matter tracts running between different brain structures, giving support to the tantalizing hypothesis that ASD is a connectivity problem where long-range connectivity is diminished in favor of increased local connectivity (Belmonte et al., 2004, Courchesne and Pierce 2005, Rippon et al., 2007, Rane et al., 2015).

Another interesting facet of the ASD literature included is the uprising trend of scanning the brains post-fixation (*ex vivo*) rather than in vivo. Despite the lack of definitive proof that one approach is superior to the other, the process of fixation does affect some properties of the tissue and can lead to significant shrinkage in the axons (Horowitz Horowitz et al., 2015) casting some doubts on the findings of such studies.

Akin to ASD, Schizophrenia (SCZ) is a multifarious disorder with presentations that differ from case to case. SCZ appears to be the product of complex intercalation between a multitude of genetic and environmental risk factors. GWAS studies identified plenty of genes to be associated with an increased risk of developing SCZ including those implicated in various vital functions such as immunity, synaptic function, and development. Various pieces of evidence point at the complicity of a faulty dopaminergic and glutamatergic neurotransmission in the genesis of the positive and the negative symptoms of SCZ, respectively (Kahn et al., 2015, Owen et al., 2016, Marder and Cannon 2019).

Administration of agents such as amphetamine or phencyclidine, that interfere with the dopaminergic or the glutamatergic pathways, was the classical way of generating animals recapitulating some of the SCZ aspects (Katsnelson 2014). In the current literature, animals treated with N-methyl-d-aspartate receptor (NMDAR) antagonists agents such as MK801 (dizocilpine) (Wu et al., 2016) or prenatally exposed to compounds such as methylazoxymethanol acetate (MAM) (Chin et al., 2011) or endotoxins such as polyinosinic:polycytidylic acid (poly I:C) (Missault et al., 2019, Di Biase et al., 2020) were used as SCZ animal models. Other transgenic models that lack essential genes such as Gclm knock-out (Gclm KO) (Corcoba et al., 2015) or express a faulty protein were also used such as *EGR3* rat model (Ma et al., 2015).

The results depicted a general pattern of diminished FA and increased RD values in all the tissues examined including the corpus callosum (Fig. 3f), the fornix, and the cingulum (Table 2). The non-conflicting results are probably emitting from the limited number of the studies conducted rather than reflecting a solid underlying dysfunction in the microstructure, since every model is mostly affected in a different manner. In addition, it should be noticed that the experimental setup chosen is quite homogeneous across the different studies, as evident from Figure 1.

Due to its global impact as a major risk factor for a wide variety of illnesses and ultimately for premature death, the consumption of alcohol and its correlation with

health problem has been for long a subject of meticulous scrutiny (Rehm et al., 2003, Ezzati et al., 2006). The deleterious effect the alcohol has on the brain tissue is very well established, and changes in the WM microstructure are widely studied employing dw-MRI.

All the studies were performed on rats, except for one study that used ferrets (Tang et al., 2018). Different studies employed different protocols to deliver various doses of alcohol, some of which were aiming at inducing chronic alcohol consumption (Vetreno et al., 2016, Luo et al., 2017), while the others were mimicking the binge drinking cases (Pfefferbaum et al., 2015). As was the case in ASD, all the studies aside from one (Tang et al., 2018) incorporated only male rats in their investigation.

As per the studies investigated, alcohol seems to affect GM tissues such as the cerebellum, the neocortex, the thalamus, and the somatosensory cortex. Some studies also found significant differences in the WM tracts including the corpus callosum and the fornix (Pfefferbaum et al., 2015, De Santis et al., 2019). The changes in the corpus callosum and the fornix seem to follow the same direction with a decrease in the FA and L1 values and an increase in the values of MD and RD (Fig. 3g and Table 2). Unlike in WM, a decrease, rather than an increase, was reported for MD values in GM tissues when alcohol esposed animals were compared to their respective control (Vetreno et al., 2016, Chen et al., 2017), although the studies used two different alcohol delivery approaches (chronic versus acute) and different experimental strategies. Although in the case of the later study, the decrease in the MD values was not progressive as the values after 2 hours of administration slightly towered over the 30 minutes after administration values before it decreased again (Chen et al., 2017).

Chen and others, using DKI in a longitudinal study, showed an initial decrease in the MK metric in the frontal lobe 30 minutes after acute administration of alcohol, followed by a significant increase two and six hours after compared to the naive control and the 30 minutes post-consumption time point (Chen et al., 2017). Besides giving credence to the sensitivity of DKI to minor changes, these results could mean that alcohol has an acute early-stage effect (Sippel 1974, Tabakoff et al., 1976) followed by a long-lasting effect (Crews et al., 2006, Crews and Nixon 2009, Kane and Drew 2016). Interestingly, in another longitudinal study, De Santis et al. reported changes in the corpus callosum and the fornix that progressed even after 6 weeks of abstinence (De Santis et al., 2019).

Stress is essentially a coping response to threats that might challenge the individual's existence and can provide an adaptation mechanism to changes that might occur in the subject's homeostasis. Chronic exposure to stress during different life stages can lead to several social abnormalities and aberrant interactions, as well as to developing depression and different forms of aggression (Lupien et al., 2009, Roozendaal et al., 2009, Sandi and Haller 2015). Rodents studies of stress seem to follow the same paradigm of using mainstream animals such as C57 mice (Grandjean et al., 2016, Liu et al., 2018b) or stress-hyper-reactive animals such as Wister Kyoto (WKY) rats (Zalsman et al., 2015, Zalsman et al., 2017). The animals were then exposed to different types of stressors for various amounts of time to mimic the state of chronic stress exposure. The stressors can vary between putting the rodent with an aggressor, wetting cage, elevated platform, or restraining. Some protocols include using more than one stressor (Hemanth Kumar et al., 2014). The animals are typically screened to test their resilience to stress experienced earlier and then categorized into anhedonic susceptible animals and resilient animals. Results indicate that indeed chronic stress can have a physical toll on the brain's microstructure. Numerous structures that are implicated in the stress response such as the hippocampus (Fig. 3h), the amygdala, and the hypothalamus were found to be affected in these studies. However, the paradigms used to induce stress varied widely between studies in addition to a wide discrepancy in the acquisition parameters which might explain the apparent contradictions. A vivid example would be the DKI results reported in some of the studies included (Delgado y Palacios et al., 2011, Khan et al., 2016, Khan et al., 2018a, Khan et al., 2018b). Despite using the same stress-inducing protocols, the findings varied substantially (Table 2). A noteworthy issue is the use of two values with only 9 directions to estimate the kurtosis tensor (Khan et al., 2018a), while the minimum requirments are 15 directions per b-value (Jensen and Helpern 2010).

Conclusions

Dw-MRI is a powerful tool to investigate microstructural abnormalities in the intact brain. Tapping the potential of such technique in preclinical investigation has the potential to boost our understanding of a multitude of disorders. However, using dw-MRI is a delicate process and requires strong knowledge of proper acquisition

parameters; in this review, we highlighted several cases in which the observed heterogeneity of the results can be at least partially explained by the experimental choice, rather than by true biological variability in the model. Future work is needed to reach a consensus on the optimal experimental scheme to be used; however, a few points can be highlighted. We encourage, whenever possible, the use of a stronger magnetic field (7-11T or higher for mice and at least 4.7T or higher for rats). If one is interested in information coming from the extracellular space, a conventional DTI sequence with b=1000 s/mm^2 and a minimum of 30 directions, as used in the majority of the studies included in this review, is recommended. For pathologies in which axonal involvement is expected, we suggest increasing the b-value range and the diffusion time to explore higher b-values and access more advanced dw-MRI models, keeping in mind that the reduction in the SNR needs to be compensated with more directions and/or more repetitions. Lastly, whenever possible, an isotropic resolution should be the first choice followed by an in-plane isotropic acquisition.

Acknowledgments: SDS was supported by the European Research Council through a Marie Skłodowska-Curie Individual Fellowship (Grant #749506) and by the Generalitat Valenciana through a Subvencion a la Excelencia de Juniors Investigadores (SEJI/2019/038). AE was supported by La Caixa-Severo Ochoa predoctoral fellowship from Obra Social La Caixa. All authors also acknowledge financial support from the Spanish State Research Agency through the Severo Ochoa Program for Centres of Excellence in R&D (SEV- 2017-0723).

Author contributions: SDS: conceptualization, supervision, visualization, writing, reviewing and editing. AE: literature search, writing, reviewing, visualization, and editing. ACC: literature search, visualization, reviewing, and editing. JL: reviewing and editing.

Conflicts of interests: The authors declare no conflicts of interests.

Table 1. Summary of the neurodegenerative studies included in the review.

Article	Disorder	Animal	Model name	Control sample size	Model sample size	Field strength	No shells	Max B-value(s/mm2)	No. directions	In vivo or ex vivo	Results in model compared to WT ↓ or ↑
Badea et al., 2016	AD	Mice	CVN-AD	8	9	9.4T	1	1595	12	Ex vivo	VBA: ↓FA; ROIs: ↓FA, ↓AD, ↑RD, ↑ADC
Thiessen et al., 2010	AD	Mice	TgCRND8	4	7	7T	8	1345	64	In vivo	ROIs: No differences
Mueggler et al., 2004	AD	Mice	APP23	5-6	8-10	7T	5	2000	N/A	In vivo	ROIs: ↓ADC
Munoz-Moreno et al., 2018	AD	Rats	TgF344-AD	9	9	7T	1	1000	60	In vivo	ROIs: ↓FA-W, ↑FD-W
Snow et al., 2017	AD	Mice	3xTg	8	7	7T	1	1000	6	In vivo	ROIs: ↓FA, ↓AD
Shu et al., 2013	AD	Mice	APP/PS1	9	9	7T	1	800	N/A	In vivo	VBA: ↑FA, ↑AD, ↑MD, ↑RD; ROIs: ↑FA, ↑AD, ↑MD, ↑RD
Qin et al., 2013	AD	Mice	APP/PS1	9	9	7T	1	800	30	In vivo	VBA: ↑FA, ↑AD, ↑MD, ↑RD; ROIs: ↑FA, ↑AD, ↑MD, ↑RD: cortex
Muller et al., 2013	AD	Mice	Tg2576	5	7	11.7T	1	1000	30	In vivo	VBA: ↑FA, ↓FA, ↓AD, ↓MD, ↓RD; ROIs: ↓FA
Praet et al., 2018	AD	Mice	APP/PS1	20	19	7T	7	2800	140	In vivo	VBA: ↓FA, ↑RD, ↑AK; ROIs: ↓FA, ↑RD, ↑AD, ↓AD, ↑MD, ↑AK, ↑MK, ↑RK
Harms et al., 2006	AD	Mice	APPsw (Tg2576)	9-10	9-10	7T	1	1890	20	Ex vivo	ROIs: ↓RA
Sun et al., 2005	AD	Mice	APPsw (Tg2576)	8	8	4.7T	1	764	6	In vivo	ROIs: ↑RD, ↓Tr, ↓AD, ↓RD, ↓RA
Kastyak-Ibrahim et al.,	AD	Mice	3xTg	3-4	8	7T	1	1034	307	In vivo ex vivo	ROIs (In vivo): No differences; ROIs (Ex

2013.											vivo): No differences
Song et al., 2004	AD	Mice	PDAPP	8-20	10-11	4.7T	1	764	6	In vivo	ROIs: ↓RA, ↑Tr, ↑RD, ↑AD
Shen et al., 2018	AD	Mice	APP/PS1	12	12	7T	1	1000	30	In vivo	ROIS: No differences
Colgan et al., 2016	AD	Mice	rTg4510	5	5	9.4T	2	2000	50	In vivo	ROIs: ↑IsoVF, ↓IsoVF, ↑NDI, ↓NDI↑MD↑FA↓FA, ↑ODI, ↓ODI
Vanhoutte et al., 2013	AD	Mice	APP/PS1	5	5	9.4T	7	2800	210	In vivo	ROIs: ↑rMK, ↑rRK, ↑rAK
Zerbi et al., 2014	AD	Mice	apoE4 apoE-KO	9-10	8-10	11.7T	1	1000	30	In vivo	VBA (apoE4): ↑MD, ↓FA; ROIs (apoE4): ↑MD, ↑AD; VBA (apoE-KO): ↑MD, ↓FA ROIs (apoE4-KO): No differences
Grandjean et al., 2014	AD	Mice	arcAβ	7-10	8-11	9.4T	1	690	36	In vivo	VBA: ↓FA; ROIs: ↓FA
Grandjean et al., 2016b	AD	Mice	arcAβ E22ΔAβ PSAPP	11-12	9-12	9.4T	1	1000	36	In vivo	VBA (arcAβ): No differences; ROIs (arcAβ); ↑FA, ↑AD,↓RD VBA (E22ΔAβ): No differences; ROIs (E22ΔAβ): No differences VBA (PSAPP): No differences; ROIs (PSAPP): ↓FA
Zerbi et al., 2013	AD	Mice	APP/PS1	15	9	11.7T	1	1000	30	In vivo	VBA: ↓FA, ↑FA, ↓MD, ↑MD, ↓AD, ↑AD, ↓RD, ↑RD; ROIs: ↓FA, ↓MD, ↑MD, ↓AD, ↑AD, ↑RD
Anckaerts et	AD	Rats	TgF344-AD	10	11	7T	1	800	60	In vivo	VBA: ↓FA, ↑FA, ↓MD,

al., 2019											↑MD, ↓AD, ↑AD, ↓RD, ↑RD; ROIs: ↓FA
Khairnar et al., 2015	PD	Mice	TNWT-61	7	7	9.4T	5	2500	150	In vivo	VBA (TBSS): ↑MK, ↑AK, ↑RK, ↓MD, ↓RD; ROIs: ↑AK, ↑RK, ↓RD, ↓MD, ↓AD, ↓RD
Khairnar et al., 2017	PD	Mice	TNWT-61	15	15	9.4T	5	2500	150	In vivo	VBA (TBSS): ↑MK, ↑AK, ↓AD; ROIs: ↑MK, ↑AK, ↑RK, ↓RD, ↑FA
Khairnar et al., 2016	PD	Mice	TNWT-61	12	9	9.4T	5	2500	150	In vivo	VBA (TBSS): ↑MK, ↑AK, ↑FA, ↓AD, ↓RD; ROIs: ↑MK, ↑AK, ↑RK, ↓MD, ↓AD, ↓RD
Arab et al., 2019	PD	Mice	METH	5-6	9-11	9.4T	5	2500	150	In vivo	VBA (TBSS): ↑FA, ↑RK, ↓MD, ↓AD, ↓RD; ROIs: ↓MK, ↓RK, ↑AD, ↑RD, ↑MK, ↓MD, ↓RD, ↑FA
Cong et al., 2016	PD	Mice	MitoPark	9	6	7T	1	1200	30	In vivo	ROIs: ↓ADC, ↓FA
Perlbarg et al., 2018	PD	Rats	6-OHDA	5	10	11.7T	1	1500	81	In vivo	ROIs: ↑FA, ↑MD, ↑AD
Ferris et al., 2018	PD	Rats	PINK1	15	15	7T	1	1000	10	In vivo	ROIs: No differences
Cai et al., 2019	PD	Rats	PINK1	10	10	7T	1	1000	10	In vivo	ROIs: ↓ADC, ↓AD, ↓RD, ↓FA
Liu et al., 2018a	PD	Rats	Rotenone 6-OHDA	6	12	3T	1	1000	15	In vivo	ROIs (Rotenone): ↓FA; ROIs (6-OHDA): ↓FA, ↑FA
Boska et al., 2007	PD	Mice	MPTP	5	5	7T	1	800	12	In vivo	ROIs: ↓FA, ↑MD, ↑AD, ↑RD
Liu et al.,	PD	Rats	Rotenone	6	12	3T	1	1000	15	In vivo	ROIs: ↓FA, ↑MD

2017											
Soria et al., 2011	PD	Rats	6-OHDA inj	4	8	7T	1	1000	30	In vivo	ROIs: ↓FA, ↓AD, ↑RD
Van Camp et al., 2009	PD	Rats	6-OHDA	4	5	7T	1	800	7	In vivo	ROIs: No differences; VBA: ↑FA; VBA-guided ROIs: ↑FA, ↓L1
Monnot et al., 2017	PD	Rats	6-OHDA	4	4	9.4T	1	1250	30	Ex vivo	VBA: ↓FA, ↑RD; ROIs: No differences
Fang et al., 2018	PD	Rats	6-OHDA	8	8	3T	1	1000	15	In vivo	ROIs: ↓FA
Blockx et al., 2012a	HD	Rats	TgHD	5-6	6	9.4T	7	2800	107	In vivo	ROIs: ↓FA, ↓MD, ↓AD, ↓RD, ↑FA, ↑MD, ↑AD, ↑RD, ↑MK, ↑AK, ↑RK, ↑KA
Blockx et al., 2012b	HD	Rats	TgHD	7	7	9.4T	7	2800	105	In vivo	ROIs: ↑FA, ↑MD, ↑AD, ↑RD, ↑KA, ↑RK
Gatto et al., 2019	HD	Mice	R6/2	3	3	17.6T	1	1500	12	Ex vivo	ROIs: ↓FA, ↑MD, ↑AD, ↑RD
Garcia-Miralles et al., 2016	HD	Mice	YAC128	7	8	7T	1	1500	30	In vivo	VBA: ↓FA; ROIs: ↓FA
Teo et al., 2016	HD	Mice Rats	YAC128 BACHD	8-13	8-14	7T	1	1500 1000	30 256	In vivo	VBA (YAC128): ↓FA; ROIs (YAC128): ↓FA; ROIs (BACHD): ↓FA
Xiang et al., 2011	HD	Mice	R6/2	3	3	11.7T	1	1500	6	Ex vivo	ROIs: ↓FA
Gatto et al., 2015	HD	Mice	YFP, R6/2	3	3	9.4T	1	1000	12	Ex vivo	ROIs: ↓FA
Antonsen et al., 2013	HD	Rats	TgHD	4	5	7T	1	800	12	Ex vivo	VBA: ↑FA, ↓MD, ↓AD, ↓RD, ↑RD; ROIs: ↑FA, ↓MD, ↓AD, ↓RD
Blockx et al., 2011	HD	Rats	TgHD	10	10	9.4T	1	800	6	In vivo	ROIs: No differences

Nishioka et al., 2017	MS	Mice	EAE	5	5	11.7T	1	850	21	In vivo	ROIs: ↓FA, ↑RD
Atkinson et al., 2019	MS	Mice	CPZ	5-6	6-8	7T 9.4T	1	1000 3000	30 30	In vivo ex vivo	ROIs (in vivo): ↓FA, ↑RD; VBA (TBSS): in vivo: ↓FA, ↑MD, ↑RD, ↑L1; ROIs (ex vivo): ↓FA
Crombe et al., 2018	MS	Mice	EAE	15	16	4.7T	2	2700	65	In vivo	ROIs: ↓MD, ↓AD
Sun et al., 2007	MS	Mice	EAE	16	16	4.7T	1	847	6	In vivo	ROIs: ↓AD, ↑RD
Planche et al., 2017	MS	Mice	EAE 2	12	12	4.7T	1	2000	30	In vivo	ROIs: ↓FA, ↑AD
Nishioka et al., 2019	MS	Mice	EAE	8	4-7	11.7T	1	850	21	In vivo	ROIs: ↓Tr, ↓FA, ↓AD, ↑RD
Boretius et al., 2012	MS	Mice	CPZ CPZ + EAE	5	5	9.4T	1	1000	12	In vivo	ROIs: ↓FA, ↓AD, ↑RD
Song et al., 2005	MS	Mice	CPZ	8	6-12	4.7T	1	1600	6	Ex vivo	ROIs: ↓RA, ↑RD, ↑Tr

Abbreviations: ↑, increase; ↓, decrease; ADC, apparent diffusion coefficient; AK, axial kurtosis; FA, fractional anisotropy; FA-W, weighted fractional anisotropy; FD-W, weighted fiber density; HD, Huntington's disease; IsoVF, isotropic volume fraction; KA, kurtosis anisotropy; KO, Knock-out; L1, axial diffusivity; MD, mean diffusivity; MK, mean kurtosis; MS, multiple sclerosis; N/A, not aplicable; NDI, neurite density; ODI, orientation dispersion index; PD, Parkinson's disease; RA, relative anisotropy; rAK, relative axial kurtosis; RD, radial diffusivity; RK, radial kurtosis; rMK, relative mean kurtosis; ROI, region of interest; rRK, relative radial kurtosis; T, tesla; TBSS, tract-based spatial statistics; Tr, trace; VBA, voxel-based analysis; WT, wild type. Sample sizes are displayed as (minimum-maximum) in cases where there are different age groups or multiple models in the same study.

Table 2. Summary of neurodevelopmental/psychiatric disorders included in the review.

Article	Disorder	Animal	Model name	Control sample size	Model sample size	Field strength	No shells	Max B-value(s/mm2)	No. directions	In vivo or ex vivo	Results in model compared to WT ↓ or ↑
Liska et al., 2017	ASD	Mice	Cntnap2$^{-/-}$	13	10	7T	1	3000	81	Ex vivo	Tractography: No differences
Zerbi et al., 2019	ASD	Mice	Fmr1$^{-/y}$	23	26	7T	2	2000	180	Ex vivo	ROIs: ↓FA, ↑RD
Wilkes et al., 2019	ASD	Mice	C58/J	10	17	17,6	2	3000	60	Ex vivo	ROIs: ↓FA, ↓AD
Kumar et al., 2012	ASD	Mice	BALB/cJ	11-12	27-28	9.4T	1	786,73	6	In vivo	ROIs (cross-sectional): ↓FA, ↑FA, ↑MD; ROIs (longitudinal): ↑FA
Ellegood et al., 2013	ASD	Mice	BTBR T+tf/J (BTBR)	12	12	7T	1	1917	30	Ex vivo	VBA: ↓FA, ↑FA; ROIs: ↓FA
Kumar et al., 2014	ASD	Mice	NL-3	7-9	5-10	9.4T	1	902	6	Ex vivo	ROIs: No differences
Ellegood et al., 2011	ASD	Mice	NL-3	8	8	7T	1	1956	6	Ex vivo	VBA: ↓FA, ↑RD; ROIs: No differences
Dodero et al., 2013	ASD	Mice	BTBR T+tf/J (BTBR)	9	9	7T	1	1262	81	Ex vivo	VBA (TBSS): ↓FA; ROIs: ↓FA
Haberl et al., 2015	ASD	Mice	Fmr1$^{-/y}$	12	7	11.7T	1	1000	30	In vivo	ROIs: ↓FA
Kumar et al., 2018	ASD	Mice	16p11.2 hemideletion (del/+)	12	9	9.4T	1	902	6	Ex vivo	VBA (TBSS): ↓FA, ↓FA

Pervolaraki et al., 2019	ASD	Mice	Nrxn2α KO	6	6	9.4T	1	1200	6	Ex vivo	ROIs: ↑FA, ↓FA, ↑AD, ↓RD, ↓ADC
Missault et al., 2019	SCZ	Rats	Poly I:C	11	10-15	7T	1	800	60	In vivo	VBA: No differences
Zhang et al., 2019	SCZ	Mice	ErbB4-KO (ErbB4-/-)	27	23	7T	1	800	30	In vivo	VBA: ↓FA
Corcoba et al., 2015	SCZ	Mice	Gclm KO	16	15	14.1T	1	1000	6	In vivo	ROIs: ↓FA, ↑RD
Ma et al., 2015	SCZ	Rats	EGR3	6	6	3T	1	1000	32	In vivo	ROIs: No differences; Fiber tracts: No differences
Chin et al., 2011	SCZ	Rats	MAM	7	4	7T	1	730	30	In vivo	ROIs: ↓FA
Di Biase et al., 2020	SCZ	Rats	Poly I:C	8	9	7T	1	1400	50	In vivo	VBA (TBSS): ↑F_W
Gimenez et al., 2017	SCZ	Mice	MAP6-KO	8	8	7T	1	1500	6	Ex vivo	No differences in transversal ADC
Wu et al., 2016	SCZ	Rats	MK801	11	12	7T	1	800	60	In vivo	VBA: ↓FA; ROIs: ↓FA, ↑MD, ↑AD, ↑RD
Vetreno et al., 2016	Alc	Rats	Intragastric	7	7	9.4T	1	N/A	12	Ex vivo	ROIs: ↑FA, ↓MD, ↓AD
Luo et al., 2017	Alc	Rats	Intragastric	10	10	7T	1	1031.7	6	In vivo	ROIs: ↓FA
Chen et al., 2017	Alc	Rats	Intragastric	5	10	7T	2	2000	60	In vivo	ROIs: ↓MK, ↑MK, ↓FA, ↑FA, ↓MD, ↑MD
Pfefferbaum et al., 2015	Alc	Rats	Intragastric	9	10	3T	1	1464	6	In vivo	VBA (TBSS): ↓FA
De Santis et al., 2019	Alc	Rats	Marchigian Sardinian	9	9-18	7T	1	1000	30	In vivo	VBA (TBSS) (1mo consumption): ↓FA, ↑MD, ↓L1, ↑RD; Fiber tracts (1 mo consumption): ↓FA,

											↑MD, ↑RD; VBA (TBSS): (2 wks): ↓FA, ↓L1; VBA (TBSS) (6 wks abistenance): ↓FA, ↓L1, ↑RD
Tang et al., 2018	Alc	Ferrets	Intraperitoneal	6	6	7T	2	4000	128	Ex vivo	ROIs: ↑FA, ↓MK, ↓AK, ↓RK
Liu et al., 2018b	Stress	Mice	CSDS	7	7-10	7T	1	1000	30	In vivo	ROIs: ↓FA, ↑MD, ↑RD
Grandjean et al., 2016a	Stress	Mice	CPS	27	26	9.4T	1	1000	36	In vivo	VBA: No differences; ROIs: ↑FA
Zalsman et al., 2017	Stress	Rats	WKY	20	20	7T	1	1000	15	In vivo	VBA: ↓FA, ↑FA, ↑MD, ↑AD, ↓AD, ↑RD Fiber tracts: ↓FA, ↑MD, ↑AD, ↑RD
Zalsman et al., 2015	Stress	Rats	WKY	22	19	7T	1	1000	15	In vivo	VBA: ↑ADC, ↓FA, ↑FA
Hemanth Kumar et al., 2014	Stress	Rats	CMS	10	10	7T	1	700	46	In vivo	ROIs: ↓FA, ↑FA, ↑MD, ↓MD, ↑AD, ↑RD
Khan et al., 2018a	Stress	Rats	CMS	8	8	9.4T	2	2500	18	In vivo	ROIs: ↑FA, ↑AD, ↑AK, ↑RK
van der Marel et al., 2013	Depression	Rats	5-HTT$^{-/-}$	11	14	4.7T	1	1250	50	In vivo	VBA (TBSS): No differences; ROIs: ↓FA: genu cc
Delgado y Palacios et al., 2011	Stress	Rats	CMS	7	7	9.4T	7	2800	210	In vivo	ROIs: ↓MK, ↓RK
Khan et al., 2016 Khan et al., 2018b	Stress	Rats	CMS	8	8	9.4	14	8000	156	Ex vivo	ROIs: ↑NDI, ↓MD, ↓$D_{eff,}$ ↓D_L

Abbreviations: ↑, increase; ↓, decrease; Deff, extracellular diffusivity; ADC, apparent diffusion coefficient; AK, axial kurtosis; Alc, Alcoholism; ASD, autism spectrum disorder; DL, intraneurite diffusivity; FA, fractional anisotropy; FA-W, weighted fractional anisotropy; FD-W, weighted fiber density; Fw, extracellular water fraction; KO, Knock-out; L1, axial diffusivity; MD, mean diffusivity; MK, mean kurtosis; mo, month; N/A, not aplicable; NDI, neurite density; RD, radial diffusivity; RK, radial kurtosis; ROI, region of interest; SCZ, schizophrenia; T, tesla; TBSS, tract-based spatial statistics; Tr, trace; VBA, xoxel-based analysis; wk, week; WT, wild type Poly I:C, polyinosinic:polycytidylic Acid; MAM, methylazoxymethanol acetate; WKY, Wistar-Kyoto strain; CMS, chronic mild stress; CPS, chronic psychosocial stress; CSDS, chronic social defeat; MK801, dizocilpine. Sample sizes are displayed as (minimum-maximum) in cases where there are different age groups or multiple models in the same study.

Bibliography:

Agosta, F., M. Pievani, S. Sala, C. Geroldi, S. Galluzzi, G. B. Frisoni and M. Filippi (2011). "White matter damage in Alzheimer disease and its relationship to gray matter atrophy." Radiology **258**(3): 853-863. doi: 10.1148/radiol.10101284

Alexander, D. C., T. B. Dyrby, M. Nilsson and H. Zhang (2019). "Imaging brain microstructure with diffusion MRI: practicality and applications." NMR Biomed **32**(4): e3841. doi: 10.1002/nbm.3841

Anckaerts, C., I. Blockx, P. Summer, J. Michael, J. Hamaide, C. Kreutzer, H. Boutin, S. Couillard-Despres, M. Verhoye and A. Van der Linden (2019). "Early functional connectivity deficits and progressive microstructural alterations in the TgF344-AD rat model of Alzheimer's Disease: A longitudinal MRI study." Neurobiol Dis **124**: 93-107. doi: 10.1016/j.nbd.2018.11.010

Antonsen, B. T., Y. Jiang, J. Veraart, H. Qu, H. P. Nguyen, J. Sijbers, S. von Horsten, G. A. Johnson and T. B. Leergaard (2013). "Altered diffusion tensor imaging measurements in aged transgenic Huntington disease rats." Brain Struct Funct **218**(3): 767-778. doi: 10.1007/s00429-012-0427-0

Ascherio, A. and M. A. Schwarzschild (2016). "The epidemiology of Parkinson's disease: risk factors and prevention." The Lancet. Neurology **15**(12): 1257-1272. doi: 10.1016/S1474-4422(16)30230-7

Assaf, Y., T. Blumenfeld-Katzir, Y. Yovel and P. J. Basser (2008). "AxCaliber: a method for measuring axon diameter distribution from diffusion MRI." Magn Reson Med **59**(6): 1347-1354. doi: 10.1002/mrm.21577

Atkinson, K. C., J. B. Lee, J. P. C. Hasselmann, S. H. Kim, A. Drew, J. Soto, J. A. Katzenellenbogen, N. G. Harris, A. Obenaus and S. K. Tiwari-Woodruff (2019). "Diffusion tensor imaging identifies aspects of therapeutic estrogen receptor beta ligand-induced remyelination in a mouse model of multiple sclerosis." Neurobiol Dis **130**: 104501. doi: 10.1016/j.nbd.2019.104501

Barrière, D. A., R. Magalhães, A. Novais, P. Marques, E. Selingue, F. Geffroy, F. Marques, J. Cerqueira, J. C. Sousa, F. Boumezbeur, M. Bottlaender, T. M. Jay, A. Cachia, N. Sousa and S. Mériaux (2019). "The SIGMA rat brain templates and atlases for multimodal MRI data analysis and visualization." Nature Communications **10**(1): 5699. doi: 10.1038/s41467-019-13575-7

Basser, P. J. (1995). "Inferring microstructural features and the physiological state of tissues from diffusion-weighted images." NMR Biomed **8**(7-8): 333-344.

Basser, P. J., J. Mattiello and D. Lebihan (1994). "Estimation of the Effective Self-Diffusion Tensor from the NMR Spin Echo." Journal of Magnetic Resonance, Series B **103**(3): 247-254. doi: https://doi.org/10.1006/jmrb.1994.1037

Bates, G. P., R. Dorsey, J. F. Gusella, M. R. Hayden, C. Kay, B. R. Leavitt, M. Nance, C. A. Ross, R. I. Scahill, R. Wetzel, E. J. Wild and S. J. Tabrizi (2015). "Huntington disease." Nature reviews. Disease primers **1**: 15005-15005. doi: 10.1038/nrdp.2015.5

Beal, M. F. (2010). "Parkinson's disease: a model dilemma." Nature **466**(7310): S8-S10. doi: 10.1038/466S8a

Belmonte, M. K., G. Allen, A. Beckel-Mitchener, L. M. Boulanger, R. A. Carper and S. J. Webb (2004). "Autism and abnormal development of brain connectivity." J Neurosci **24**(42): 9228-9231. doi: 10.1523/JNEUROSCI.3340-04.2004

Blockx, I., G. De Groof, M. Verhoye, J. Van Audekerke, K. Raber, D. Poot, J. Sijbers, A. P. Osmand, S. Von Horsten and A. Van der Linden (2012a). "Microstructural changes observed with DKI in a transgenic Huntington rat model: evidence for abnormal neurodevelopment." Neuroimage **59**(2): 957-967. doi: 10.1016/j.neuroimage.2011.08.062

Blockx, I., N. Van Camp, M. Verhoye, R. Boisgard, A. Dubois, B. Jego, E. Jonckers, K. Raber, K. Siquier, B. Kuhnast, F. Dolle, H. P. Nguyen, S. Von Horsten, B. Tavitian and A. Van der Linden (2011). "Genotype specific age related changes in a transgenic rat model of Huntington's disease." Neuroimage **58**(4): 1006-1016. doi: 10.1016/j.neuroimage.2011.07.007

Blockx, I., M. Verhoye, J. Van Audekerke, I. Bergwerf, J. X. Kane, Y. P. R. Delgado, J. Veraart, B. Jeurissen, K. Raber, S. von Horsten, P. Ponsaerts, J. Sijbers, T. B. Leergaard and A. Van der Linden (2012b). "Identification and characterization of Huntington related pathology: an in vivo DKI imaging study." Neuroimage **63**(2): 653-662. doi: 10.1016/j.neuroimage.2012.06.032

Boretius, S., A. Escher, T. Dallenga, C. Wrzos, R. Tammer, W. Bruck, S. Nessler, J. Frahm and C. Stadelmann (2012). "Assessment of lesion pathology in a new animal model of MS by multiparametric MRI and DTI." Neuroimage **59**(3): 2678-2688. doi: 10.1016/j.neuroimage.2011.08.051

Chen, X. R., J. Y. Zeng, Z. W. Shen, L. M. Kong and W. B. Zheng (2017). "Diffusion Kurtosis Imaging Detects Microstructural Changes in the Brain after Acute Alcohol Intoxication in Rats." Biomed Res Int **2017**: 4757025. doi: 10.1155/2017/4757025

Chin, C. L., P. Curzon, A. J. Schwartz, E. M. O'Connor, L. E. Rueter, G. B. Fox, M. Day and A. M. Basso (2011). "Structural abnormalities revealed by magnetic resonance

imaging in rats prenatally exposed to methylazoxymethanol acetate parallel cerebral pathology in schizophrenia." Synapse **65**(5): 393-403. doi: 10.1002/syn.20857

Chyi, T. and C. Chang (1999). "Temporal evolution of 3-nitropropionic acid-induced neurodegeneration in the rat brain by T2-weighted, diffusion-weighted, and perfusion magnetic resonance imaging." Neuroscience **92**(3): 1035-1041. doi: 10.1016/s0306-4522(99)00076-7

Colgan, N., B. Siow, J. M. O'Callaghan, I. F. Harrison, J. A. Wells, H. E. Holmes, O. Ismail, S. Richardson, D. C. Alexander, E. C. Collins, E. M. Fisher, R. Johnson, A. J. Schwarz, Z. Ahmed, M. J. O'Neill, T. K. Murray, H. Zhang and M. F. Lythgoe (2016). "Application of neurite orientation dispersion and density imaging (NODDI) to a tau pathology model of Alzheimer's disease." Neuroimage **125**: 739-744. doi: 10.1016/j.neuroimage.2015.10.043

Cong, L., E. R. Muir, C. Chen, Y. Qian, J. Liu, K. C. Biju, R. A. Clark, S. Li and T. Q. Duong (2016). "Multimodal MRI Evaluation of the MitoPark Mouse Model of Parkinson's Disease." PLoS One **11**(3): e0151884. doi: 10.1371/journal.pone.0151884

Corcoba, A., P. Steullet, J. M. Duarte, Y. Van de Looij, A. Monin, M. Cuenod, R. Gruetter and K. Q. Do (2015). "Glutathione Deficit Affects the Integrity and Function of the Fimbria/Fornix and Anterior Commissure in Mice: Relevance for Schizophrenia." Int J Neuropsychopharmacol **19**(3): pyv110. doi: 10.1093/ijnp/pyv110

Courchesne, E. and K. Pierce (2005). "Why the frontal cortex in autism might be talking only to itself: local over-connectivity but long-distance disconnection." Curr Opin Neurobiol **15**(2): 225-230. doi: 10.1016/j.conb.2005.03.001

Crews, F., K. Nixon, D. Kim, J. Joseph, B. Shukitt-Hale, L. Qin and J. Zou (2006). "BHT blocks NF-kappaB activation and ethanol-induced brain damage." Alcohol Clin Exp Res **30**(11): 1938-1949. doi: 10.1111/j.1530-0277.2006.00239.x

Crews, F. T. and K. Nixon (2009). "Mechanisms of neurodegeneration and regeneration in alcoholism." Alcohol Alcohol **44**(2): 115-127. doi: 10.1093/alcalc/agn079

Crombe, A., V. Planche, G. Raffard, J. Bourel, N. Dubourdieu, A. Panatier, H. Fukutomi, V. Dousset, S. Oliet, B. Hiba and T. Tourdias (2018). "Deciphering the microstructure of hippocampal subfields with in vivo DTI and NODDI: Applications to experimental multiple sclerosis." Neuroimage **172**: 357-368. doi: 10.1016/j.neuroimage.2018.01.061

Curran, K. M., L. Emsell and A. Leemans (2016). Quantitative DTI Measures. Diffusion Tensor Imaging: A Practical Handbook. W. Van Hecke, L. Emsell and S. Sunaert. New York, NY, Springer New York**:** 65-87.

De Santis, S., P. Bach, L. Perez-Cervera, A. Cosa-Linan, G. Weil, S. Vollstadt-Klein, D. Hermann, F. Kiefer, P. Kirsch, R. Ciccocioppo, W. H. Sommer and S. Canals (2019). "Microstructural White Matter Alterations in Men With Alcohol Use Disorder and Rats With Excessive Alcohol Consumption During Early Abstinence." JAMA Psychiatry **76**(7): 749-758. doi: 10.1001/jamapsychiatry.2019.0318

De Santis, S., T. Granberg, R. Ouellette, C. A. Treaba, F. Qiuyun, E. Herranz, C. Mainero and N. Toschi (2017). "Early axonal damage in normal appearing white matter in multiple sclerosis: Novel insights from multi-shell diffusion MRI." Conf Proc IEEE Eng Med Biol Soc **2017**: 3024-3027. doi: 10.1109/EMBC.2017.8037494

Delgado y Palacios, R., A. Campo, K. Henningsen, M. Verhoye, D. Poot, J. Dijkstra, J. Van Audekerke, H. Benveniste, J. Sijbers, O. Wiborg and A. Van der Linden (2011). "Magnetic resonance imaging and spectroscopy reveal differential hippocampal changes in anhedonic and resilient subtypes of the chronic mild stress rat model." Biol Psychiatry **70**(5): 449-457. doi: 10.1016/j.biopsych.2011.05.014

Di Biase, M. A., G. Katabi, Y. Piontkewitz, S. Cetin-Karayumak, I. Weiner and O. Pasternak (2020). "Increased extracellular free-water in adult male rats following in utero exposure to maternal immune activation." Brain Behav Immun **83**: 283-287. doi: 10.1016/j.bbi.2019.09.010

Dodero, L., M. Damiano, A. Galbusera, A. Bifone, S. A. Tsaftsaris, M. L. Scattoni and A. Gozzi (2013). "Neuroimaging Evidence of Major Morpho-Anatomical and Functional Abnormalities in the BTBR T+TF/J Mouse Model of Autism." PLOS ONE **8**(10): e76655. doi: 10.1371/journal.pone.0076655

Drummond, E. and T. Wisniewski (2017). "Alzheimer's disease: experimental models and reality." Acta Neuropathol **133**(2): 155-175. doi: 10.1007/s00401-016-1662-x

Ellegood, J., J. P. Lerch and R. M. Henkelman (2011). "Brain abnormalities in a Neuroligin3 R451C knockin mouse model associated with autism." Autism Res **4**(5): 368-376. doi: 10.1002/aur.215

Emsell, L., W. Van Hecke and J.-D. Tournier (2016). Introduction to Diffusion Tensor Imaging. Diffusion Tensor Imaging: A Practical Handbook. W. Van Hecke, L. Emsell and S. Sunaert. New York, NY, Springer New York**:** 7-19.

Ezzati, M., S. V. Hoorn, A. D. Lopez, G. Danaei, A. Rodgers, C. D. Mathers and C. J. L. Murray (2006). Comparative Quantification of Mortality and Burden of Disease Attributable to Selected Risk Factors. Global Burden of Disease and Risk Factors. A. D. Lopez, C. D. Mathers, M. Ezzati, D. T. Jamison and C. J. L. Murray. Washington (DC).

Fang, Y., T. Zheng, L. Liu, D. Gao, Q. Shi, Y. Dong and D. Du (2018). "Role of the combination of FA and T2* parameters as a new diagnostic method in therapeutic evaluation of parkinson's disease." J Magn Reson Imaging **48**(1): 84-93. doi: 10.1002/jmri.25900

Ferris, C. F., T. R. Morrison, S. Iriah, S. Malmberg, P. Kulkarni, J. C. Hartner and M. Trivedi (2018). "Evidence of Neurobiological Changes in the Presymptomatic PINK1 Knockout Rat." J Parkinsons Dis **8**(2): 281-301. doi: 10.3233/jpd-171273

Filippi, M., A. Bar-Or, F. Piehl, P. Preziosa, A. Solari, S. Vukusic and M. A. Rocca (2018). "Multiple sclerosis." Nature reviews. Disease primers **4**(1): 43-43. doi: 10.1038/s41572-018-0041-4

Garcia-Miralles, M., X. Hong, L. J. Tan, N. S. Caron, Y. Huang, X. V. To, R. Y. Lin, S. Franciosi, S. Papapetropoulos, L. Hayardeny, M. R. Hayden, K. H. Chuang and M. A. Pouladi (2016). "Laquinimod rescues striatal, cortical and white matter pathology and results in modest behavioural improvements in the YAC128 model of Huntington disease." Sci Rep **6**: 31652. doi: 10.1038/srep31652

Gatto, R. G., A. Q. Ye, L. Colon-Perez, T. H. Mareci, A. Lysakowski, S. D. Price, S. T. Brady, M. Karaman, G. Morfini and R. L. Magin (2019). "Detection of axonal degeneration in a mouse model of Huntington's disease: comparison between diffusion tensor imaging and anomalous diffusion metrics." Magma **32**(4): 461-471. doi: 10.1007/s10334-019-00742-6

Grandjean, J., D. Azzinnari, A. Seuwen, H. Sigrist, E. Seifritz, C. R. Pryce and M. Rudin (2016). "Chronic psychosocial stress in mice leads to changes in brain functional connectivity and metabolite levels comparable to human depression." Neuroimage **142**: 544-552. doi: 10.1016/j.neuroimage.2016.08.013

Hagmann, P., L. Jonasson, P. Maeder, J. P. Thiran, V. J. Wedeen and R. Meuli (2006). "Understanding diffusion MR imaging techniques: from scalar diffusion-weighted imaging to diffusion tensor imaging and beyond." Radiographics **26 Suppl 1**: S205-223. doi: 10.1148/rg.26si065510

Harms, M. P., J. J. Kotyk and K. M. Merchant (2006). "Evaluation of white matter integrity in ex vivo brains of amyloid plaque-bearing APPsw transgenic mice using magnetic resonance diffusion tensor imaging." Exp Neurol **199**(2): 408-415. doi: 10.1016/j.expneurol.2006.01.002

Hemanth Kumar, B. S., S. K. Mishra, R. Trivedi, S. Singh, P. Rana and S. Khushu (2014). "Demyelinating evidences in CMS rat model of depression: a DTI study at 7 T." Neuroscience **275**: 12-21. doi: 10.1016/j.neuroscience.2014.05.037

Horowitz, A., D. Barazany, I. Tavor, G. Yovel and Y. Assaf (2015). "Response to the comments on the paper by Horowitz et al. (2014)." Brain structure & function **220**(3): 1791-1792. doi: 10.1007/s00429-015-1031-x

Huettel, S. A., A. W. Song and G. McCarthy (2014). Functional Magnetic Resonance Imaging, Sinauer.

Iossifov, I., B. J. O'Roak, S. J. Sanders, M. Ronemus, N. Krumm, D. Levy, H. A. Stessman, K. T. Witherspoon, L. Vives, K. E. Patterson, J. D. Smith, B. Paeper, D. A. Nickerson, J. Dea, S. Dong, L. E. Gonzalez, J. D. Mandell, S. M. Mane, M. T. Murtha, C. A. Sullivan, M. F. Walker, Z. Waqar, L. Wei, A. J. Willsey, B. Yamrom, Y.-h. Lee, E. Grabowska, E. Dalkic, Z. Wang, S. Marks, P. Andrews, A. Leotta, J. Kendall, I. Hakker, J. Rosenbaum, B. Ma, L. Rodgers, J. Troge, G. Narzisi, S. Yoon, M. C. Schatz, K. Ye, W. R. McCombie, J. Shendure, E. E. Eichler, M. W. State and M. Wigler (2014). "The contribution of de novo coding mutations to autism spectrum disorder." Nature **515**: 216. doi: 10.1038/nature13908
https://www.nature.com/articles/nature13908 - supplementary-information

Janke, A. L. and J. F. Ullmann (2015). "Robust methods to create ex vivo minimum deformation atlases for brain mapping." Methods **73**: 18-26. doi: 10.1016/j.ymeth.2015.01.005

Jensen, J. H., M. F. Falangola, C. Hu, A. Tabesh, O. Rapalino, C. Lo and J. A. Helpern (2011). "Preliminary observations of increased diffusional kurtosis in human brain following recent cerebral infarction." NMR Biomed **24**(5): 452-457. doi: 10.1002/nbm.1610

Jensen, J. H. and J. A. Helpern (2010). "MRI quantification of non-Gaussian water diffusion by kurtosis analysis." NMR in biomedicine **23**(7): 698-710. doi: 10.1002/nbm.1518

Jensen, J. H., J. A. Helpern, A. Ramani, H. Lu and K. Kaczynski (2005). "Diffusional kurtosis imaging: the quantification of non-gaussian water diffusion by means of magnetic resonance imaging." Magn Reson Med **53**(6): 1432-1440. doi: 10.1002/mrm.20508

Jones, D. K. (2010). Diffusion MRI, Oxford University Press.

Jones, D. K. and P. J. Basser (2004). ""Squashing peanuts and smashing pumpkins": how noise distorts diffusion-weighted MR data." Magnetic resonance in medicine **52**(5): 979-993. doi: 10.1002/mrm.20283

Kahn, R. S., I. E. Sommer, R. M. Murray, A. Meyer-Lindenberg, D. R. Weinberger, T. D. Cannon, M. O'Donovan, C. U. Correll, J. M. Kane, J. van Os and T. R. Insel (2015).

"Schizophrenia." Nature reviews. Disease primers **1**: 15067-15067. doi: 10.1038/nrdp.2015.67

Kane, C. J. and P. D. Drew (2016). "Inflammatory responses to alcohol in the CNS: nuclear receptors as potential therapeutics for alcohol-induced neuropathologies." J Leukoc Biol **100**(5): 951-959. doi: 10.1189/jlb.3MR0416-171R

Katsnelson, A. (2014). "Drug development: The modelling challenge." Nature **508**(7494): S8-S9. doi: 10.1038/508S8a

Khairnar, A., P. Latta, E. Drazanova, J. Ruda-Kucerova, N. Szabo, A. Arab, B. Hutter-Paier, D. Havas, M. Windisch, A. Sulcova, Z. Starcuk, Jr. and I. Rektorova (2015). "Diffusion Kurtosis Imaging Detects Microstructural Alterations in Brain of alpha-Synuclein Overexpressing Transgenic Mouse Model of Parkinson's Disease: A Pilot Study." Neurotox Res **28**(4): 281-289. doi: 10.1007/s12640-015-9537-9

Khairnar, A., J. Ruda-Kucerova, E. Drazanova, N. Szabo, P. Latta, A. Arab, B. Hutter-Paier, D. Havas, M. Windisch, A. Sulcova, Z. Starcuk, Jr., A. Kiraly and I. Rektorova (2016). "Late-stage alpha-synuclein accumulation in TNWT-61 mouse model of Parkinson's disease detected by diffusion kurtosis imaging." J Neurochem **136**(6): 1259-1269. doi: 10.1111/jnc.13500

Khairnar, A., J. Ruda-Kucerova, N. Szabo, E. Drazanova, A. Arab, B. Hutter-Paier, J. Neddens, P. Latta, Z. Starcuk, Jr. and I. Rektorova (2017). "Early and progressive microstructural brain changes in mice overexpressing human alpha-Synuclein detected by diffusion kurtosis imaging." Brain Behav Immun **61**: 197-208. doi: 10.1016/j.bbi.2016.11.027

Khan, A. R., A. Chuhutin, O. Wiborg, C. D. Kroenke, J. R. Nyengaard, B. Hansen and S. N. Jespersen (2016). "Biophysical modeling of high field diffusion MRI demonstrates micro-structural aberration in chronic mild stress rat brain." Neuroimage **142**: 421-430. doi: 10.1016/j.neuroimage.2016.07.001

Khan, A. R., B. Hansen, O. Wiborg, C. D. Kroenke and S. N. Jespersen (2018a). "Diffusion MRI and MR spectroscopy reveal microstructural and metabolic brain alterations in chronic mild stress exposed rats: A CMS recovery study." Neuroimage **167**: 342-353. doi: 10.1016/j.neuroimage.2017.11.053

Khan, A. R., C. D. Kroenke, O. Wiborg, A. Chuhutin, J. R. Nyengaard, B. Hansen and S. N. Jespersen (2018b). "Differential microstructural alterations in rat cerebral cortex in a model of chronic mild stress depression." PLoS One **13**(2): e0192329. doi: 10.1371/journal.pone.0192329

Kingsley, P. B. (2006). "Introduction to diffusion tensor imaging mathematics: Part I. Tensors, rotations, and eigenvectors." Concepts in Magnetic Resonance Part A **28A**(2): 101-122. doi: 10.1002/cmr.a.20048

Kumar, M., J. T. Duda, W. T. Hwang, C. Kenworthy, R. Ittyerah, S. Pickup, E. S. Brodkin, J. C. Gee, T. Abel and H. Poptani (2014). "High resolution magnetic resonance imaging for characterization of the neuroligin-3 knock-in mouse model associated with autism spectrum disorder." PLoS One **9**(10): e109872. doi: 10.1371/journal.pone.0109872

Kumar, M., S. Kim, S. Pickup, R. Chen, A. H. Fairless, R. Ittyerah, T. Abel, E. S. Brodkin and H. Poptani (2012). "Longitudinal in-vivo diffusion tensor imaging for assessing brain developmental changes in BALB/cJ mice, a model of reduced sociability relevant to autism." Brain Res **1455**: 56-67. doi: 10.1016/j.brainres.2012.03.041

Kumar, V. J., N. M. Grissom, S. E. McKee, H. Schoch, N. Bowman, R. Havekes, M. Kumar, S. Pickup, H. Poptani, T. M. Reyes, M. Hawrylycz, T. Abel and T. Nickl-Jockschat (2018). "Linking spatial gene expression patterns to sex-specific brain structural changes on a mouse model of 16p11.2 hemideletion." Transl Psychiatry **8**(1): 109. doi: 10.1038/s41398-018-0157-z

Le Bihan, D. and E. Breton (1985). "Imagerie de diffusion in-vivo par résonance magnétique nucléaire." Comptes-Rendus de l'Académie des Sciences **93**(5): 27-34.

Liu, L. X., D. Du, Z. Q. Wang, Y. Fang, T. Zheng, Y. C. Dong, Q. L. Shi, M. Zhao, F. Xiao and J. Du (2018a). "Differences in brain pathological changes between rotenone and 6-hydroxydopamine Parkinson's disease models." Neural Regen Res **13**(7): 1276-1280. doi: 10.4103/1673-5374.235076

Liu, L. X., D. Du, T. Zheng, Y. Fang, Y. S. Chen, H. L. Yi, Q. Y. He, D. W. Gao and Q. L. Shi (2017). "Detecting dopaminergic neuronal degeneration using diffusion tensor imaging in a rotenone-induced rat model of Parkinson's disease: fractional anisotropy and mean diffusivity values." Neural Regen Res **12**(9): 1485-1491. doi: 10.4103/1673-5374.213559

Liu, X., J. Yuan, Y. Guang, X. Wang and Z. Feng (2018b). "Longitudinal in vivo Diffusion Tensor Imaging Detects Differential Microstructural Alterations in the Hippocampus of Chronic Social Defeat Stress-Susceptible and Resilient Mice." Front Neurosci **12**: 613. doi: 10.3389/fnins.2018.00613

Lu, H., J. H. Jensen, A. Ramani and J. A. Helpern (2006). "Three-dimensional characterization of non-gaussian water diffusion in humans using diffusion kurtosis imaging." NMR Biomed **19**(2): 236-247. doi: 10.1002/nbm.1020

Luo, J., Z. Shen, G. Chen, D. Wang and X. Yu (2017). "Pontine Changes in Metabolites and Axonal Fibres of Rats Following Four-week Alcohol Exposure: In Vivo Diffusion Tensor Imaging and 1h-magnetic Resonance Spectroscopy Study at 7.0 T." Alcohol Alcohol **52**(2): 145-150. doi: 10.1093/alcalc/agw087

Lupien, S. J., B. S. McEwen, M. R. Gunnar and C. Heim (2009). "Effects of stress throughout the lifespan on the brain, behaviour and cognition." Nat Rev Neurosci **10**(6): 434-445. doi: 10.1038/nrn2639

Ma, E., T. Song, H. Zhang, J. Lu, L. Wang, Q. Zhao, R. Guo, M. Li, G. Ma, G. Lu and K. Li (2015). "The reduction of volume and fiber bundle connections in the hippocampus of EGR3 transgenic schizophrenia rats." Neuropsychiatr Dis Treat **11**: 1625-1638. doi: 10.2147/ndt.S81440

Marder, S. R. and T. D. Cannon (2019). "Schizophrenia." The New England journal of medicine **381**(18): 1753-1761. doi: 10.1056/NEJMra1808803

Miles, J. H. (2011). "Autism spectrum disorders—A genetics review." Genetics In Medicine **13**: 278. doi: 10.1097/GIM.0b013e3181ff67ba

Missault, S., C. Anckaerts, S. Ahmadoun, I. Blockx, M. Barbier, K. Bielen, D. Shah, S. Kumar-Singh, W. H. De Vos, A. Van der Linden, S. Dedeurwaerdere and M. Verhoye (2019). "Hypersynchronicity in the default mode-like network in a neurodevelopmental animal model with relevance for schizophrenia." Behav Brain Res **364**: 303-316. doi: 10.1016/j.bbr.2019.02.040

Monnot, C., X. Zhang, S. Nikkhou-Aski, P. Damberg and P. Svenningsson (2017). "Asymmetric dopaminergic degeneration and levodopa alter functional corticostriatal connectivity bilaterally in experimental parkinsonism." Exp Neurol **292**: 11-20. doi: 10.1016/j.expneurol.2017.02.014

Munoz-Moreno, E., R. Tudela, X. Lopez-Gil and G. Soria (2018). "Early brain connectivity alterations and cognitive impairment in a rat model of Alzheimer's disease." Alzheimers Res Ther **10**(1): 16. doi: 10.1186/s13195-018-0346-2

Nalls, M. A., N. Pankratz, C. M. Lill, C. B. Do, D. G. Hernandez, M. Saad, A. L. DeStefano, E. Kara, J. Bras, M. Sharma, C. Schulte, M. F. Keller, S. Arepalli, C. Letson, C. Edsall, H. Stefansson, X. Liu, H. Pliner, J. H. Lee, R. Cheng, C. International Parkinson's Disease Genomics, G. I. Parkinson's Study Group Parkinson's Research: The Organized, andMe, GenePd, C. NeuroGenetics Research, G. Hussman Institute of Human, I. Ashkenazi Jewish Dataset, H. Cohorts for, E. Aging Research in Genetic, C. North American Brain Expression, C. United Kingdom Brain Expression, C. Greek Parkinson's Disease, G. Alzheimer Genetic Analysis, M. A. Ikram, J. P. A. Ioannidis, G. M. Hadjigeorgiou, J. C. Bis, M. Martinez, J. S. Perlmutter, A. Goate, K. Marder, B.

Fiske, M. Sutherland, G. Xiromerisiou, R. H. Myers, L. N. Clark, K. Stefansson, J. A. Hardy, P. Heutink, H. Chen, N. W. Wood, H. Houlden, H. Payami, A. Brice, W. K. Scott, T. Gasser, L. Bertram, N. Eriksson, T. Foroud and A. B. Singleton (2014). "Large-scale meta-analysis of genome-wide association data identifies six new risk loci for Parkinson's disease." Nature genetics **46**(9): 989-993. doi: 10.1038/ng.3043

Nishioka, C., H. F. Liang, B. Barsamian and S. W. Sun (2019). "Sequential phases of RGC axonal and somatic injury in EAE mice examined using DTI and OCT." Mult Scler Relat Disord **27**: 315-323. doi: 10.1016/j.msard.2018.11.010

Nishioka, C., H. F. Liang, C. F. Chung and S. W. Sun (2017). "Disease stage-dependent relationship between diffusion tensor imaging and electrophysiology of the visual system in a murine model of multiple sclerosis." Neuroradiology **59**(12): 1241-1250. doi: 10.1007/s00234-017-1904-1

Oguz, I., M. S. McMurray, M. Styner and J. M. Johns (2012). "The translational role of diffusion tensor image analysis in animal models of developmental pathologies." Dev Neurosci **34**(1): 5-19. doi: 10.1159/000336825

Owen, M. J., A. Sawa and P. B. Mortensen (2016). "Schizophrenia." Lancet (London, England) **388**(10039): 86-97. doi: 10.1016/S0140-6736(15)01121-6

Perlbarg, V., J. Lambert, B. Butler, M. Felfli, R. Valabregue, A. L. Privat, S. Lehericy and A. Petiet (2018). "Alterations of the nigrostriatal pathway in a 6-OHDA rat model of Parkinson's disease evaluated with multimodal MRI." PLoS One **13**(9): e0202597. doi: 10.1371/journal.pone.0202597

Pervolaraki, E., A. L. Tyson, F. Pibiri, S. L. Poulter, A. C. Reichelt, R. J. Rodgers, S. J. Clapcote, C. Lever, L. C. Andreae and J. Dachtler (2019). "The within-subject application of diffusion tensor MRI and CLARITY reveals brain structural changes in Nrxn2 deletion mice." Mol Autism **10**: 8. doi: 10.1186/s13229-019-0261-9

Pfefferbaum, A., N. M. Zahr, D. Mayer, T. Rohlfing and E. V. Sullivan (2015). "Dynamic responses of selective brain white matter fiber tracts to binge alcohol and recovery in the rat." PLoS One **10**(4): e0124885. doi: 10.1371/journal.pone.0124885

Poewe, W., K. Seppi, C. M. Tanner, G. M. Halliday, P. Brundin, J. Volkmann, A.-E. Schrag and A. E. Lang (2017). "Parkinson disease." Nature reviews. Disease primers **3**: 17013-17013. doi: 10.1038/nrdp.2017.13

Praet, J., N. V. Manyakov, L. Muchene, Z. Mai, V. Terzopoulos, S. de Backer, A. Torremans, P. J. Guns, T. Van De Casteele, A. Bottelbergs, B. Van Broeck, J. Sijbers, D. Smeets, Z. Shkedy, L. Bijnens, D. J. Pemberton, M. E. Schmidt, A. Van der Linden and M. Verhoye (2018). "Diffusion kurtosis imaging allows the early detection and

longitudinal follow-up of amyloid-beta-induced pathology." Alzheimers Res Ther **10**(1): 1. doi: 10.1186/s13195-017-0329-8

Qin, Y. Y., M. W. Li, S. Zhang, Y. Zhang, L. Y. Zhao, H. Lei, K. Oishi and W. Z. Zhu (2013). "In vivo quantitative whole-brain diffusion tensor imaging analysis of APP/PS1 transgenic mice using voxel-based and atlas-based methods." Neuroradiology **55**(8): 1027-1038. doi: 10.1007/s00234-013-1195-0

Rane, P., D. Cochran, S. M. Hodge, C. Haselgrove, D. N. Kennedy and J. A. Frazier (2015). "Connectivity in Autism: A Review of MRI Connectivity Studies." Harv Rev Psychiatry **23**(4): 223-244. doi: 10.1097/HRP.0000000000000072

Rehm, J., R. Room, K. Graham, M. Monteiro, G. Gmel and C. T. Sempos (2003). "The relationship of average volume of alcohol consumption and patterns of drinking to burden of disease: an overview." Addiction **98**(9): 1209-1228. doi: 10.1046/j.1360-0443.2003.00467.x

Rice, J. (2012). "Animal models: Not close enough." Nature **484**(7393): S9-S9. doi: 10.1038/nature11102

Richards, K., C. Watson, R. F. Buckley, N. D. Kurniawan, Z. Yang, M. D. Keller, R. Beare, P. F. Bartlett, G. F. Egan, G. J. Galloway, G. Paxinos, S. Petrou and D. C. Reutens (2011). "Segmentation of the mouse hippocampal formation in magnetic resonance images." Neuroimage **58**(3): 732-740. doi: 10.1016/j.neuroimage.2011.06.025

Rippon, G., J. Brock, C. Brown and J. Boucher (2007). "Disordered connectivity in the autistic brain: challenges for the "new psychophysiology"." Int J Psychophysiol **63**(2): 164-172. doi: 10.1016/j.ijpsycho.2006.03.012

Roozendaal, B., B. S. McEwen and S. Chattarji (2009). "Stress, memory and the amygdala." Nat Rev Neurosci **10**(6): 423-433. doi: 10.1038/nrn2651

Sandi, C. and J. Haller (2015). "Stress and the social brain: behavioural effects and neurobiological mechanisms." Nat Rev Neurosci **16**(5): 290-304. doi: 10.1038/nrn3918

Scheltens, P., K. Blennow, M. M. B. Breteler, B. de Strooper, G. B. Frisoni, S. Salloway and W. M. Van der Flier (2016). "Alzheimer's disease." Lancet (London, England) **388**(10043): 505-517. doi: 10.1016/S0140-6736(15)01124-1

Shu, N., Z. Wang, Z. Qi, K. Li and Y. He (2011). "Multiple diffusion indices reveals white matter degeneration in Alzheimer's disease and mild cognitive impairment: a

tract-based spatial statistics study." J Alzheimers Dis **26 Suppl 3**: 275-285. doi: 10.3233/JAD-2011-0024

Shu, X., Y. Y. Qin, S. Zhang, J. J. Jiang, Y. Zhang, L. Y. Zhao, D. Shan and W. Z. Zhu (2013). "Voxel-based diffusion tensor imaging of an APP/PS1 mouse model of Alzheimer's disease." Mol Neurobiol **48**(1): 78-83. doi: 10.1007/s12035-013-8418-6

Sippel, H. W. (1974). "The acetaldehyde content in rat brain during ethanol metabolism." J Neurochem **23**(2): 451-452. doi: 10.1111/j.1471-4159.1974.tb04380.x

Small, S. A. and K. Duff (2008). "Linking Abeta and tau in late-onset Alzheimer's disease: a dual pathway hypothesis." Neuron **60**(4): 534-542. doi: 10.1016/j.neuron.2008.11.007

Snow, W. M., R. Dale, Z. O'Brien-Moran, R. Buist, D. Peirson, M. Martin and B. C. Albensi (2017). "In Vivo Detection of Gray Matter Neuropathology in the 3xTg Mouse Model of Alzheimer's Disease with Diffusion Tensor Imaging." J Alzheimers Dis **58**(3): 841-853. doi: 10.3233/jad-170136

Song, S. K., J. Yoshino, T. Q. Le, S. J. Lin, S. W. Sun, A. H. Cross and R. C. Armstrong (2005). "Demyelination increases radial diffusivity in corpus callosum of mouse brain." Neuroimage **26**(1): 132-140. doi: 10.1016/j.neuroimage.2005.01.028

Stahl, R., O. Dietrich, S. J. Teipel, H. Hampel, M. F. Reiser and S. O. Schoenberg (2007). "White matter damage in Alzheimer disease and mild cognitive impairment: assessment with diffusion-tensor MR imaging and parallel imaging techniques." Radiology **243**(2): 483-492. doi: 10.1148/radiol.2432051714

Stejskal, E. O. and J. E. Tanner (1965). "Spin Diffusion Measurements: Spin Echoes in the Presence of a Time-Dependent Field Gradient." The Journal of Chemical Physics **42**(1): 288-292. doi: 10.1063/1.1695690

Sun, S. W., H. F. Liang, R. E. Schmidt, A. H. Cross and S. K. Song (2007). "Selective vulnerability of cerebral white matter in a murine model of multiple sclerosis detected using diffusion tensor imaging." Neurobiol Dis **28**(1): 30-38. doi: 10.1016/j.nbd.2007.06.011

Sun, S. W., S. K. Song, M. P. Harms, S. J. Lin, D. M. Holtzman, K. M. Merchant and J. J. Kotyk (2005). "Detection of age-dependent brain injury in a mouse model of brain amyloidosis associated with Alzheimer's disease using magnetic resonance diffusion tensor imaging." Exp Neurol **191**(1): 77-85. doi: 10.1016/j.expneurol.2004.09.006

Tabakoff, B., R. A. Anderson and R. F. Ritzmann (1976). "Brain acetaldehyde after ethanol administration." Biochem Pharmacol **25**(11): 1305-1309. doi: 10.1016/0006-2952(76)90094-0

Tang, S., S. Xu, R. P. Gullapalli and A. E. Medina (2018). "Effects of Early Alcohol Exposure on Functional Organization and Microstructure of a Visual-Tactile Integrative Circuit." Alcohol Clin Exp Res **42**(4): 727-734. doi: 10.1111/acer.13611

Teo, R. T., X. Hong, L. Yu-Taeger, Y. Huang, L. J. Tan, Y. Xie, X. V. To, L. Guo, R. Rajendran, A. Novati, C. Calaminus, O. Riess, M. R. Hayden, H. P. Nguyen, K. H. Chuang and M. A. Pouladi (2016). "Structural and molecular myelination deficits occur prior to neuronal loss in the YAC128 and BACHD models of Huntington disease." Hum Mol Genet **25**(13): 2621-2632. doi: 10.1093/hmg/ddw122

Ullmann, J. F., C. Watson, A. L. Janke, N. D. Kurniawan, G. Paxinos and D. C. Reutens (2014). "An MRI atlas of the mouse basal ganglia." Brain Struct Funct **219**(4): 1343-1353. doi: 10.1007/s00429-013-0572-0

Ullmann, J. F., C. Watson, A. L. Janke, N. D. Kurniawan and D. C. Reutens (2013). "A segmentation protocol and MRI atlas of the C57BL/6J mouse neocortex." Neuroimage **78**: 196-203. doi: 10.1016/j.neuroimage.2013.04.008

Vanhoutte, G., S. Pereson, Y. P. R. Delgado, P. J. Guns, B. Asselbergh, J. Veraart, J. Sijbers, M. Verhoye, C. Van Broeckhoven and A. Van der Linden (2013). "Diffusion kurtosis imaging to detect amyloidosis in an APP/PS1 mouse model for Alzheimer's disease." Magn Reson Med **69**(4): 1115-1121. doi: 10.1002/mrm.24680

Vetreno, R. P., R. Yaxley, B. Paniagua and F. T. Crews (2016). "Diffusion tensor imaging reveals adolescent binge ethanol-induced brain structural integrity alterations in adult rats that correlate with behavioral dysfunction." Addict Biol **21**(4): 939-953. doi: 10.1111/adb.12232

Wheeler-Kingshott, C. A. M. and M. Cercignani (2009). "About "axial" and "radial" diffusivities." Magnetic resonance in medicine **61**(5): 1255-1260. doi: 10.1002/mrm.21965

Wilkes, B. J., C. Bass, H. Korah, M. Febo and M. H. Lewis (2019). "Volumetric magnetic resonance and diffusion tensor imaging of C58/J mice: neural correlates of repetitive behavior." Brain Imaging Behav. doi: 10.1007/s11682-019-00158-9

Wu, H., X. Wang, Y. Gao, F. Lin, T. Song, Y. Zou, L. Xu and H. Lei (2016). "NMDA receptor antagonism by repetitive MK801 administration induces schizophrenia-like structural changes in the rat brain as revealed by voxel-based morphometry and

diffusion tensor imaging." Neuroscience **322**: 221-233. doi: 10.1016/j.neuroscience.2016.02.043

Xiang, Z., M. Valenza, L. Cui, V. Leoni, H. K. Jeong, E. Brilli, J. Zhang, Q. Peng, W. Duan, S. A. Reeves, E. Cattaneo and D. Krainc (2011). "Peroxisome-proliferator-activated receptor gamma coactivator 1 alpha contributes to dysmyelination in experimental models of Huntington's disease." J Neurosci **31**(26): 9544-9553. doi: 10.1523/jneurosci.1291-11.2011

Zalsman, G., A. Gutman, L. Shbiro, R. Rosenan, J. J. Mann and A. Weller (2015). "Genetic vulnerability, timing of short-term stress and mood regulation: A rodent diffusion tensor imaging study." Eur Neuropsychopharmacol **25**(11): 2075-2085. doi: 10.1016/j.euroneuro.2015.08.006

Zalsman, G., A. Weller, L. Shbiro, R. Barzilay, A. Gutman, A. Weizman, J. J. Mann, J. Wasserman and D. Wasserman (2017). "Fibre tract analysis using diffusion tensor imaging reveals aberrant connectivity in a rat model of depression." World J Biol Psychiatry **18**(8): 615-623. doi: 10.1080/15622975.2016.1190866

Zerbi, V., M. Kleinnijenhuis, X. Fang, D. Jansen, A. Veltien, J. Van Asten, N. Timmer, P. J. Dederen, A. J. Kiliaan and A. Heerschap (2013). "Gray and white matter degeneration revealed by diffusion in an Alzheimer mouse model." Neurobiol Aging **34**(5): 1440-1450. doi: 10.1016/j.neurobiolaging.2012.11.017

Zerbi, V., M. Markicevic, F. Gasparini, A. Schroeter, M. Rudin and N. Wenderoth (2019). "Inhibiting mGluR5 activity by AFQ056/Mavoglurant rescues circuit-specific functional connectivity in Fmr1 knockout mice." Neuroimage **191**: 392-402. doi: 10.1016/j.neuroimage.2019.02.051

Zhang, H., T. Schneider, C. A. Wheeler-Kingshott and D. C. Alexander (2012). "NODDI: practical in vivo neurite orientation dispersion and density imaging of the human brain." Neuroimage **61**(4): 1000-1016. doi: 10.1016/j.neuroimage.2012.03.072

Zhang, Y., N. Schuff, G. H. Jahng, W. Bayne, S. Mori, L. Schad, S. Mueller, A. T. Du, J. H. Kramer, K. Yaffe, H. Chui, W. J. Jagust, B. L. Miller and M. W. Weiner (2007). "Diffusion tensor imaging of cingulum fibers in mild cognitive impairment and Alzheimer disease." Neurology **68**(1): 13-19. doi: 10.1212/01.wnl.0000250326.77323.01